LUND UNIVERSITY
Faculty of Science

Quantum teleportation of single-electron states

Edvin Olofsson

Thesis submitted for the degree of Master of Science
Project duration: 4 months

Supervised by Peter Samuelsson and Patrick Potts

Department of Physics
Division of Mathematical Physics
May 2019

Abstract

Quantum teleportation is a way to transfer a quantum state between two locations, by utilizing a shared entangled state, measurements and the ability to communicate measurement outcomes between the two locations. This thesis consists of a theoretical investigation of an experiment that would implement quantum teleportation using single-electron states in mesoscopic architectures. First, we studied an idealized version, where it is assumed that single-electron states can be detected, which is yet to be demonstrated for certain types of implementations. There we find a teleportation efficiency of 25% or 12.5%, depending on whether a conditional unitary operation can be applied to the teleported state. We also show how to verify successful teleportation, by describing a way to perform state tomography on the teleported state. Next, we considered a more realistic setup where single-electron states called levitons are periodically injected. We show that at $T = 0$ it is possible to perform state tomography using measurements of low-frequency current correlators up to order three. This opens the possibility to perform teleportation experiments that do not rely on single-electron detection. The correlators were calculated within the framework of Floquet scattering theory. Strictly speaking, the simple picture of single-electron state teleportation breaks down at finite temperatures. However, we find that the generalized observables can be interpreted in terms of noisy teleportation.

Acknowledgments

I want to thank my supervisors Patrick Potts and Peter Samuelsson for providing me with a very interesting topic for my thesis, and for the help they have given me throughout, both with the physics side of things and with the writing of my thesis. I would also like to thank the other people in C367 for the good atmosphere in the office. Finally, I want to thank my family for all the love and support that they have given me over the course of this project and my time in Lund.

Contents

List of Figures

List of Tables

List of abbreviations

2DEG Two-dimensional electron gas

NMR Nuclear magnetic resonance

POVM Positive operator valued measure

QHE Quantum Hall effect

QPC Quantum point contact

SAW Surface acoustic wave

Chapter 1

Introduction

Teleportation, transferring objects between different locations without physically transporting them, has long been a feature of science fiction stories. The idea does have a science fiction feel to it, so it might seem a little surprising that in 1993 it was realized by Bennett *et al.* that something analogous can take place in the realm of quantum mechanics [1]. They showed that it is possible to transfer the quantum state of a particle from one location to another, by utilizing the correlations that exist between entangled particles. The first step is to perform specific measurements on the original state and one half of an entangled state. By sending classical information about the measurement outcome to where the other half of the entangled state is located, the original state can be recovered there by performing a unitary transformation that is determined by the measurement outcome. In this context, classical information means something that can be represented using standard bits on a computer. The states that were considered in [1] are known as qubits, and are built from superpositions of two basis states. Qubits serve as the fundamental building blocks of quantum computers, and teleportation could therefore be used to transfer qubit states between different quantum computers.

There are a number of different applications of quantum teleportation within the field of quantum information. One example is to use teleportation to transfer quantum information between quantum computers, as suggested above. Quantum teleportation cannot lead to faster than light communication between the involved parties, since the protocol relies on transferring classical information between two locations, and classical signals are limited by the speed of light. By a slight modification to the teleportation scheme, it is possible to perform entanglement swapping which enables the generation of entanglement between physically separated locations with no direct link between the locations [2, 3]. Entanglement swapping is a crucial part of a quantum repeater, a protocol that can generate entanglement over long distances by using ancillary entanlged pairs and repeated entanglement swapping [4]. This could be used to extend the range of existing teleportation protocols, by increasing the distance over which entalged states can be shared [3]. It has also been demonstrated that it is possible to build a quantum computer where the qubit operations are performed using teleportation [5, 6].

Quantum teleportation is not only interesting for its technological applications, but when viewed from a quantum information theory perspective it shows that entanglement should be thought of as a useful resource. It also shows that there can exist a relationship between classical information, in this case the measurement outcomes, and quantum information, i.e. the state of a qubit. Specifically, teleportation demonstrates that two parties having a two-bit classical information channel together with a shared entangled

state can be equivalent to them having a quantum information channel, i.e. a way of directly transferring the original state between the parties [1, 7].

Successful teleportation of the polarization states of photons was reported in 1997 [8]. Since then, quantum teleportation has been performed using a variety of systems. Some examples are photonic qubits [9, 10], trapped ions [11], nuclear spins [12] and solid state qubits [13]. The distance over which states can be teleported varies greatly for the different techniques, with nuclear magnetic resonance (NMR) teleportation working on a typical distance on the order of 1 Å [3], while photon polarizations were teleported between a ground station and an orbiting satellite in 2017 [14].

Although distance is one of the parameters that is interesting to consider when comparing different teleportation schemes, it is also important to consider the efficiency of the different alternatives. The efficiency quantifies the success probability of a teleportation scheme. According to the original teleportation proposal an efficiency of 100% is possible [1], but different implementations have different efficiencies. If we again compare NMR teleportation with the teleportation of polarization qubits, we find that NMR can in principle have a success rate of 100% [12], while for photonic polarization qubits the maximum efficiency is 50%, due to restrictions in the measurement [3]. Therefore, depending on how one wishes to apply quantum teleportation, it will be necessary to consider if a high efficiency or a long range is a more important feature. This suggests a need to study different approaches to quantum teleportation in order to find their advantages and disadvantages.

This thesis aims to investigate a teleportation approach that uses spatial modes of single electrons as the qubits we wish to teleport and as the entanglement resource. The focus will be on a theoretical demonstration of teleportation using single-electron states, a determination of the efficiency, and suggestions for experimental verification. The motivation behind this approach to teleportation is that on the mesoscopic and nanometer scales there are electronic analogs to optical components such as beamsplitters, phase shifters and waveguides that can be used to manipulate single electrons. Phase shifting can be performed with magnetic fields and the role of beamsplitters is taken by quantum point contacts (QPC), which act as tunnel barriers for the electrons. The chiral edge states of the integer quantum Hall effect (QHE) function as one-dimensional and backscattering-free electronic waveguides. This field is called electron quantum optics [15]. There have been recent advances in single-electron sources that have fueled an interest in this field as a means to perform quantum information processing tasks [16]. In this thesis the focus will be on a type of source that uses Lorentzian voltage pulses applied to metallic contacts to create single-electron states called levitons. Teleportation requires a way to generate entangled states on demand and this can be achieved using electron quantum optics [17]. It was shown in [18] that if an electron in a chiral edge state scatters on a QPC the resulting superposition should be viewed as an entangled state. This will be the method used for entanglement generation in this thesis.

As we will see in Secs. 2.1 and 3.1, quantum teleportation experiments require the ability to prepare qubits in specific states, generate entangled states, perform accurate measurements in specific bases and manipulating qubits based on measurement outcomes. These operations are fundamental ingredients of quantum information and quantum computing [7]. Performing a quantum teleportation experiment using electron quantum optics can therefore serve as an indicator for how well suited electron quantum optics is for use in quantum information applications, or more generally how well such systems can be controlled. Such an experiment can also give insight into how enviromental effects impact

the performance of electron quantum optics systems in quantum information processing tasks.

The rest of this thesis is structured as follows. After the theoretical tools used in this work have been discussed, the teleportation setup that will be considered is presented and it will be demonstrated that teleportation can take place in that system. The system will be analyzed by a scattering matrix formalism [19], neglecting Coulomb interactions. Then, a positive operator-valued measure (POVM) describing an idealized electron mode detection used in the teleportation scheme will be defined. With the help of the POVM it will be possible to calculate both the probability for teleportation to succeed and the post-measurement states at the receiving location.

Next we will discuss an experiment that can verify that teleportation has taken place. The scheme is based on performing state tomography on the state at the receiving location, after the original measurement has taken place. This is done by performing measurements that probe the density matrix of the received state. First, we will discuss an idealized experiment that requires reliable single-electron detection. While there has been progress towards such detectors, they do not currently exist for the experimental architecture based on QHE edge states and levitons considered here [16]. Instead, it will be shown that using a periodic driving voltage and measuring zero frequency average currents and current correlators of second and third order it is possible to experimentally verify that teleportation takes place in the system. This line of thinking follows closely the scheme presented in [18] for detection of single-electron entanglement. It should be noted that an architecture where both single-electron sources and detectors are available does exist. In this approach, where an electron surfs on a surface acoustic wave (SAW), sufficient coherence times have not yet been reported and the approach is not considered here.

Because of the periodicity of the driving voltages, the relevant quantities can be calculated within the framework of Floquet scattering theory [19]. The calculations that deal with observable quantities will be carried out in two steps. First, we will consider the system at zero temperature where a rigorous correspondence between observable quantities in the single-shot regime and the periodically driven case can be found. This correspondence will be considered in the light of the leviton quasiparticle that is created by periodic voltage pulses.

Afterwards, the periodically driven case will be considered at non-zero temperatures. While finite temperatures spoil the ideal picture of teleporting isolated single-particle states, observables are still expected to show signatures of teleportation. More precisely, we can interpret the results as describing a noisy teleportation process, although it should be pointed out that the connection to teleportation is not completely rigorous. The calculations at non-zero temperature will also be performed using Floquet scattering theory.

Chapter 2

Background

This chapter contains the background material that is necessary to understand teleportation and how it has been treated in this thesis. It also contains the different theoretical tools that are needed to analyze the systems considered in the thesis, as well as the tools needed to perform calculations of states and relevant quantities. Section 2.1 will give a more quantitative look at teleportation than the one presented in Chapter 1. That will be followed by some background information about qubits in Section 2.2 and a description of generalized measurements in quantum mechanics in Section 2.3. Then we will discuss electron quantum optics, which is a framework that relies on electronic analogs of optical components, in Section 2.4. Section 2.5 provides a description of the scattering theory formalism that was used to analyze the teleportation setup. Section 2.5.1 introduces second quantization and the concept of a scattering matrix, while Section 2.5.2 introduces the Floquet scattering theory formalism that was used to perform calculations when we consider a system driven by periodic voltages both at zero and non-zero temperatures. Lastly, Section 2.6 presents the quasiparticles called levitons which are created by Lorentzian voltage pulses. The levitons will be useful for the interpretation of the results that are obtained for the periodically driven teleportation setup, since the driving voltage will be a train of Lorentzian pulses.

2.1 Quantum Teleportation

The basic idea of how to teleport a quantum state was introduced in Chapter 1. The aim of this section is to provide a more in depth description of what teleportation is and how it can be achieved. The original idea is due to Bennett *et al.* [1] and the version presented here is based on [20]. Figure 2.1 provides a schematic view of the teleporation protocol.

Assume that Alice has been given some unknown qubit state as an input

$$|\psi\rangle_{\mathrm{A}_0} = \alpha\,|0\rangle_{\mathrm{A}_0} + \beta\,|1\rangle_{\mathrm{A}_0}\,, \tag{2.1}$$

where A_0 labels the subsystem. Suppose also that Alice and Bob are each in possession of one half of the state

$$\left|\Phi^+\right\rangle_{\mathrm{A}_1\mathrm{B}} = \frac{1}{\sqrt{2}}\left(|00\rangle + |11\rangle\right)_{\mathrm{A}_1\mathrm{B}}\,, \tag{2.2}$$

where A_1 is the subsystem belonging to Alice and B is the subsystem belonging to Bob. This is an entangled state, which means that it cannot be written as a product of two

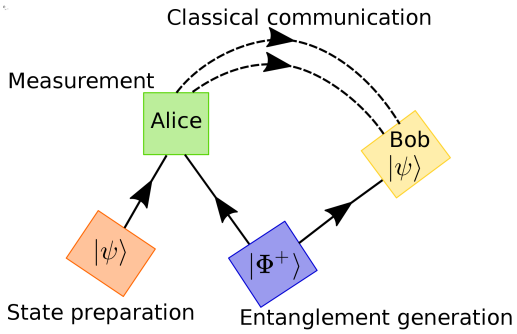

Figure 2.1: Alice and Bob are each given one half of an entangled state. Alice also receives an unknown qubit state. She performs a measurement on the combined state of the qubit and her part of the entangled state. After the measurement, she sends the result to Bob. Based on the measurement outcome, he can perform a unitary operation on his part of the entangled state and recover the unknown qubit.

single-particle states. The combined state of the three subsystems can be expressed as

$$|\phi\rangle = |\psi\rangle_{\mathrm{A}_0} \left|\Phi^+\right\rangle_{\mathrm{A}_1\mathrm{B}} = \frac{1}{\sqrt{2}}\Big(\alpha\,|000\rangle + \alpha\,|011\rangle + \beta\,|100\rangle + \beta\,|111\rangle\Big). \tag{2.3}$$

Alice then makes a measurement on the combined $\mathrm{A}_0\mathrm{A}_1$ system in the basis

$$\begin{aligned} \left|\Psi^\pm\right\rangle_{\mathrm{A}} &= \frac{1}{\sqrt{2}}\left(|01\rangle \pm |10\rangle\right)_{\mathrm{A}_0\mathrm{A}_1}, \\ \left|\Phi^\pm\right\rangle_{\mathrm{A}} &= \frac{1}{\sqrt{2}}\left(|00\rangle \pm |11\rangle\right)_{\mathrm{A}_0\mathrm{A}_1}. \end{aligned} \tag{2.4}$$

To see what the outcomes of the measurement will be, the combined state can be expressed in this basis

$$\begin{aligned} |\phi\rangle = \frac{1}{2}\Big(&\left|\Phi^+\right\rangle_{\mathrm{A}}(\alpha\,|0\rangle_{\mathrm{B}} + \beta\,|1\rangle_{\mathrm{B}}) + \left|\Phi^-\right\rangle_{\mathrm{A}}(\alpha\,|0\rangle_{\mathrm{B}} - \beta\,|1\rangle_{\mathrm{B}}) + \\ &+ \left|\Psi^+\right\rangle_{\mathrm{A}}(\beta\,|0\rangle_{\mathrm{B}} + \alpha\,|1\rangle_{\mathrm{B}}) + \left|\Psi^-\right\rangle_{\mathrm{A}}(-\beta\,|0\rangle_{\mathrm{B}} + \alpha\,|1\rangle_{\mathrm{B}})\Big). \end{aligned} \tag{2.5}$$

The possibilities for Bob's post-measurement state are

$$\begin{aligned} &\alpha\,|0\rangle_{\mathrm{B}} + \beta\,|1\rangle_{\mathrm{B}}, \\ &\alpha\,|0\rangle_{\mathrm{B}} - \beta\,|1\rangle_{\mathrm{B}}, \\ &\beta\,|0\rangle_{\mathrm{B}} + \alpha\,|1\rangle_{\mathrm{B}}, \\ -&\beta\,|0\rangle_{\mathrm{B}} + \alpha\,|1\rangle_{\mathrm{B}}. \end{aligned} \tag{2.6}$$

Each of these states is related to $|\psi\rangle_{\mathrm{A}_0}$ by a unitary transformation, although in the first case the transformation would just be the identity since it is identical to the input state. Since the form of the unitary transformation depends on the outcome of Alice's measurement, Bob can recover $|\psi\rangle$ at his location if Alice communicates the outcome of her measurement, and he is able to apply the correct transformation to his post-measurement state. Alice has then been able to transfer the input state to Bob using only entanglement and classical communication. There are four possible messages that Alice needs to send to Bob, which can be accomplished by two classical bits.

As has been pointed out in ref. [20], successful teleportation of $|\psi\rangle$ depends on whether Alice can gain any knowledge of $|\psi\rangle$ when she carries out her measurement. If we consider the example that has been described here, we see that the probabilities of Alice's measurement outcomes are all equal to $1/4$ and thus independent of $|\psi\rangle$. Her post-measurement state does therefore not contain any information about $|\psi\rangle$. However, if Alice had chosen to perform her measurement in the original basis, then an outcome of say $|00\rangle$ means that she can infer $\alpha \neq 0$. If such a basis is used, then the only possible post-measurement states for Bob is $|0\rangle$ and $|1\rangle$, and this cannot be transformed into $|\psi\rangle$ with only knowledge of Alice's measurement result, unless $|\psi\rangle$ is one of those two states. When the results of single-electron teleportation are presented later, we will see that teleportation will not be successful when Alice gains information about $|\psi\rangle$ in the course of her measurement.

The results of this section shows that a shared entangled state and a classical channel can be considered equivalent to a communications channel that directly transfers quantum information [7]. In other words, two classical bits, which is enough to communicate the measurement outcome, and one shared entangled state is equivalent to one qubit of quantum information. Since Alice and Bob share an entangled state, they are in a sense already linked by a quantum channel, but one does not require that this channel can send arbitrary qubit states, as one would of a proper quantum channel. The entangled state does not have to be generated by either Alice or Bob, but it can instead be created by a third party which sends them their halves of the state.

Another important thing to note is that we cannot teleport arbitrary states if the state that is shared between Alice and Bob is not entangled, since if that were the case one would have for the total state of all three systems

$$|\psi\rangle = |\psi\rangle_{\mathrm{A}} |\psi\rangle_{\mathrm{B}}, \tag{2.7}$$

and Bob's post-measurement state would be independent of Alice's measurement outcome. It turns out that it is only possible to achieve 100% efficiency if the shared state is of the form

$$\frac{1}{\sqrt{2}} \left(|a\rangle_{\mathrm{A}_1} |c\rangle_{\mathrm{B}} + |b\rangle_{\mathrm{A}_1} |d\rangle_{\mathrm{B}} \right), \tag{2.8}$$

where $\{|a\rangle, |b\rangle\}$ and $\{|c\rangle, |d\rangle\}$ are pairs of mutually orthonormal states [1].

2.2 Qubits

It is often very convenient to represent the state of a qubit by its density matrix ρ. One can show that any qubit density matrix can be written in the form [7]

$$\rho = \frac{I + \vec{r} \cdot \vec{\sigma}}{2}, \tag{2.9}$$

where I is the 2×2 identity matrix, $\vec{\sigma} = (\sigma_x, \sigma_y, \sigma_z)$ are the Pauli matrices and $\vec{r}$ is a vector in $\mathbb{R}^3$ with $\|\vec{r}\| \leq 1$. The components of $\vec{r}$ are given by

$$r_i = \mathrm{Tr}\,(\sigma_i \rho) = \langle \sigma_i \rangle. \tag{2.10}$$

$\vec{r}$ can be used to visualize the state of the qubit by drawing it in $\mathbb{R}^3$. The surface $\|\vec{r}\| = 1$ is called the Bloch sphere and $\vec{r}$ is called the Bloch vector. Figure 2.2 shows an illustration of how one represents qubit states on the Bloch sphere.

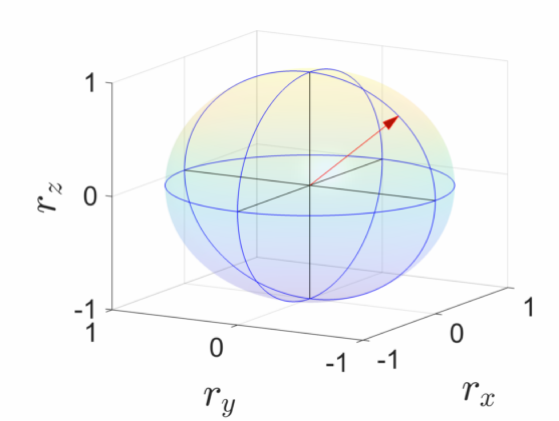

Figure 2.2: This figure shows how a pure qubit state can be represented on the Bloch sphere. The vector in the figure represents a state with Bloch vector $\vec{r} = \frac{1}{\sqrt{2}}(0, -1, 1)$.

A density matrix that is given as the outer product of a single state is called pure, since the state is known with complete certainty. If no such representation exists, then the state is said to be mixed. An important quantity that relates to this concept is the purity γ of a quantum state. γ is defined as

$$\gamma = \mathrm{Tr}\left(\rho^2\right), \tag{2.11}$$

and one can show that $0 \leq \gamma \leq 1$, with $\gamma = 1$ if and only if ρ represents a pure state [7]. A direct calculation using the representation in Eq. (2.9) shows that the purity of a qubit state is given by

$$\gamma = \frac{1 + \|\vec{r}\,\|^2}{2}. \tag{2.12}$$

ρ therefore represents a pure state precisely when $\|\vec{r}\,\| = 1$. This means that the Bloch sphere contains all possible pure states of a qubit.

When discussing how well a specific implementation of quantum teleportation performs, it seems reasonable to ask how much Bob's state resembles the original state. A quantity that can be used to represent how close two quantum states ρ_1, ρ_2 are to each other is the fidelity $\mathcal{F}$. For two qubits ρ_1, ρ_2 with Bloch vectors $\vec{r}_1$, $\vec{r}_2$ the fidelity takes the form

$$\mathcal{F} = \frac{1}{2}\left(1 + \vec{r}_1 \cdot \vec{r}_2 + \left[\left(1 - \|\vec{r}_1\,\|^2\right)\left(1 - \|\vec{r}_2\,\|^2\right)\right]^{1/2}\right), \tag{2.13}$$

as shown in ref. [21]. The fidelity is bounded between 0 and 1, and is equal to 1 precisely when $\rho_1 = \rho_2$ [21]. What is often considered for quantum teleportation experiments is the teleportation fidelity $\mathcal{F}_{\mathrm{tel}}$, which is the fidelity of the input and output states averaged over all possible input states [3]. A classical version of teleportation could be that Alice directly measures the input state in the regular $|0\rangle$, $|1\rangle$ basis and sends the result to Bob for him to prepare as the output state. One can show that the teleportation fidelity will be 2/3 and it turns out that this is the best one can do classically. That value is therefore used as a benchmark value for $\mathcal{F}_{\mathrm{tel}}$ since a value over this limit indicates that quantum resources are utilized [3].

2.3 Generalized measurements

In standard quantum mechanics courses, measurements are usually discussed in terms of projective measurements. In a projective measurement of an observable X, the possible measurement outcomes are the eigenvalues of X and the state of the system after the measurement has taken place, the post-measurement state, is the corresponding eigenstate. However, not every imaginable measurement that can be performed on a quantum system can be described as a projective measurement on only that system. Consider for instance the case of counting the number of photons of a certain energy. One way this could be done is by absorbing the photons, but this means that the number of photons before and after the measurement has changed. This in turn means that the measurement has moved the state between two different eigenspaces of the photon number operator and the measurement is therefore not projective. A more general theory for measurements in quantum mechanics is formulated in terms of Kraus operators and positive operator-valued measures (POVM). Projective measurements can then be seen as a special case of the general theory. The usefulness of the POVM formalism, is partly due to the fact that it is possible to discuss non-projective measurements and partly due to making it possible to make statements about measurement outcomes without specifying exactly how the measurement is performed.

A general measurement in quantum mechanics is described by a set of measurement outcomes $\{x\}$ and associated Kraus operators $\{M_x\}$ [7]. If the state prior to the measurement is $|\psi\rangle$, then the outcome x occurs with probability

$$p(x) = \langle\psi| M_x^\dagger M_x |\psi\rangle , \tag{2.14}$$

and the post-measurement state is given by

$$\frac{M_x}{\sqrt{p(x)}} |\psi\rangle . \tag{2.15}$$

For $p(x)$ to be a probability distribution we require

$$\sum_x p(x) = 1, \tag{2.16}$$

for all states $|\psi\rangle$ in the Hilbert space. This requirement is equivalent to

$$\sum_x M_x^\dagger M_x = I. \tag{2.17}$$

If one is working with density matrices instead of state vectors then the probabilities are calculated as

$$p(x) = \mathrm{Tr}\left(M_x \rho M_x^\dagger\right) = \mathrm{Tr}\left(M_x^\dagger M_x \rho\right), \tag{2.18}$$

while the post-measurement state for outcome x is

$$\frac{1}{p(x)} M_x \rho M_x^\dagger. \tag{2.19}$$

A POVM is defined as a set of positive operators $\{E_x\}$ satisfying the completeness relation

$$\sum_x E_x = I. \tag{2.20}$$

A linear operator A is positive if $\langle\psi| A |\psi\rangle \geq 0$ for all $|\psi\rangle$. It can be shown that all positive operators are Hermitian and that $A^\dagger A$ is positive for any A. With these definitions we see that the operators $\left\{M_x^\dagger M_x\right\}$ defined above satisfy the definition of a POVM. Note that for a set of unitary operators $\{U_x\}$ the set $\{\tilde{M}_x^\dagger \tilde{M}_x\}$ with $\tilde{M}_x = U_x M_x$ defines the same POVM as $\left\{M_x^\dagger M_x\right\}$. From the definition of a POVM we can see that

$$p(x) = \langle\psi| E_x |\psi\rangle , \tag{2.21}$$

and

$$p(x) = \mathrm{Tr}\left(E_x \rho\right), \tag{2.22}$$

should be considered probability distributions, i.e. they are positive and sum to one. In general, having only knowledge of the POVM describing a measurement will not provide enough information to determine the post-measurement state of the system. However, for our purposes it will suffice to define a POVM for mode detection of electrons in order to determine Bob's state following Alice's measurement. Let $\{M(X)\}$ be a set of Kraus operators describing Alice's measurement. Since this measurement is only performed at Alice's location, the action of $M(X)$ on the combined state of Alice and Bob is given by $M(X) \otimes I_\mathrm{B}$. Bob's post-measurement state is written in terms of a reduced density matrix

$$\rho_\mathrm{B}(X) = \frac{1}{p(X)} \mathrm{Tr}_\mathrm{A}\left(\left(M(X) \otimes I_\mathrm{B}\right) \rho \left(M^\dagger(X) \otimes I_\mathrm{B}\right)\right). \tag{2.23}$$

Here we have introduced the partial trace Tr_A over the states in Alice's subsystem, which is defined by

$$\mathrm{Tr}_\mathrm{A}\left(|\mathrm{A}\rangle \langle\mathrm{A}'| \otimes |\mathrm{B}\rangle \langle\mathrm{B}'|\right) = \mathrm{Tr}\left(|\mathrm{A}\rangle \langle\mathrm{A}'|\right) |\mathrm{B}\rangle \langle\mathrm{B}'| , \tag{2.24}$$

with $|\mathrm{A}\rangle$, $\langle\mathrm{A}'|$ arbitrary states in the A space and $|\mathrm{B}\rangle$, $\langle\mathrm{B}'|$ arbitrary states in the B space [7]. It is extended to other operators by linearity. By expanding ρ in a basis for the operators acting on the combined Hilbert spaces of Alice and Bob one can show that Eq. (2.23) reduces to

$$\rho_\mathrm{B}(X) = \frac{1}{p(X)} \mathrm{Tr}_\mathrm{A}\left(\left(E(X) \otimes I_\mathrm{B}\right) \rho\right). \tag{2.25}$$

This shows that it suffices to work with the POVM describing Alice's measurement if only Bob's post-measurement state is important.

Another property of the partial trace that will be useful is that if M is an observable on Bob's system, then

$$\mathrm{Tr}\left(M \,\mathrm{Tr}_\mathrm{A}(\rho)\right) = \mathrm{Tr}\left((I_\mathrm{A} \otimes M)\rho\right). \tag{2.26}$$

This implies that we can compute expectation values for observables on a subsystem by considering either $\mathrm{Tr}_\mathrm{A}(\rho)$ or the full density matrix ρ [7].

2.4 Electron quantum optics

The teleportation setup that will be treated in this thesis has natural analogies with optical systems. This is because the components that make up the system can be seen as electronic analogs of optical components. There are single-electron sources that emit single-electron states that we wish to control. It is also possible to treat the chiral edge states of the integer quantum Hall effect as one-dimensional waveguides for electrons. Quantum point contacts can be treated as beamsplitters, and magnetic fluxes can be used to manipulate phase differences for different electron paths. We would also like to detect the presence of single electrons with some kind of single-electron detector. This section will provide a short review of these components.

2.4.1 Single-electron sources

One important component of electron quantum optics experiments is the single-electron source. Four important single-electron sources are the mesoscopic capacitor, the single-electron pump, leviton sources and surface acoustic wave (SAW) sources [16].

Leviton sources generate a single electron excitation above the Fermi sea. This is done by applying short Lorentzian voltage pulses to metallic contacts. The resulting excitation is known as a leviton. This single-electron source will play a large role in this thesis and is discussed in more detail in Section 2.6.

The mesoscopic capacitor is a quantum dot which is tunnel coupled to a conductor. It is operated by raising the highest occupied level of the dot above the Fermi energy of the conductor so that an electron is emitted. The levels of the dot are then returned to their original heights, causing an electron to be captured by the dot and creating a hole state in the conductor. Continuous operation thus results in a stream of alternating electrons and holes.

A single-electron pump consists of a quantum dot where the height of one potential barrier can be dynamically controlled, while the other remains static. The controllable barrier is first set to a low height so that electrons can enter the dot. It is then raised so that electrons are captured in the dot, but some of them will tunnel out. The goal is to only have one electron left in the dot after this stage. The barrier is then raised further and eventually the potential at the edges of the barrier will be so large that the remaining electrons tunnel through the static barrier. Electrons generated by this source typically have high energies and it is not clear to what extent relaxation processes will negatively impact the distance over which they can be considered to be coherent [16, 22].

The SAW single-electron source uses the piezo-electric properties of for instance gallium arsenide to create an electric field moving along the surface of the GaAs substrate. The first step is to have a single-electron located in a quantum dot. Then, a pulse of soundwaves is directed towards the quantum dot, generating a traveling electric field due to the piezo-electric effect. If the pulse has sufficient amplitude, it can remove the electron from the dot and trap the electron in a minimum of the wave, essentially forming a moving quantum dot. The electron will follow along with the wave, thus enabling single-electron transport, if one can control the propagation of the wave.

2.4.2 Chiral edge states

Chiral edge states appear in the integer quantum Hall effect. The integer quantum Hall effect is observed for two-dimensional electron gases (2DEG), such as gallium arsenide heterostructures, when they are subjected to strong magnetic fields perpendicular to the sample. This will essentially cause the electrons in the bulk of the sample to perform localized circular orbits, while the confining potential at the edge of the sample will allow electrons close to the edge to travel over longer distances [23]. As the name suggests, the edge states are localized at the edges of a sample and this localization means that the states can effectively be treated as one-dimensional. The word chiral is referring to the fact that the edge states travel only along one direction for each edge of the sample. States on opposite edges travel in opposite directions. This makes edge states particularly interesting since backscattering would require them to scatter to the opposite edge of the sample. If the sample is sufficiently wide, scattering across the sample will be strongly suppressed and this process can be neglected [24]. Due to the presence of the magnetic field, the electrons in the bulk of the material will form flat energy bands called Landau

levels and the edge states arise when the confining potential change the energy of states close to the edge [23]. There will also be a splitting of these bands due to the Zeeman effect which means that, we can treat the edge states as spin polarized if we only consider the edge states belonging to a single Landau level [23].

2.4.3 Quantum point contacts

Quantum point contacts (QPC) are objects that can act as beamsplitters for chiral edge states. A QPC is a pair of contacts that have been deposited onto the surface of the sample, with a typical separation on the order of a few hundred nanometers. Applying a negative voltage to the contacts will create a repulsion barrier. If an electron is passed through a 50/50 beamsplitter the resulting state is entangled [18], which will be one of the purposes for QPCs in the teleportation setup. The entangled state will be of the form

$$|\Phi\rangle = \frac{1}{\sqrt{2}}(i\,|1\rangle_r\,|0\rangle_t + |0\rangle_r\,|1\rangle_t), \tag{2.27}$$

where r and t denote the reflected and transmitted modes, respectively. The i factor of the first term comes from the scattering matirx of the QPC, which will be introduced in Ch. 3. $|\Phi\rangle$ is an entangled state of a single particle, where the entanglement is between two subspaces of a single-particle Hilbert space [25]. It is not an entangled state of two particles, which is perhaps a more familiar notion, where the entanglement is between the Hilbert spaces of two different particles. Demonstrating that a state of the form above should be viewed as entangled is done in ref. [18], where it is shown that such states can be used to violate a Bell-type inequality. Another purpose for a QPC is to help generate the input state for teleportation by creating superpositions of transmitted and reflected electron modes.

2.4.4 Single-electron detectors

Since it is possible to generate single-electron states, a natural question to ask is whether it is possible to then detect their presence. Since teleportation relies on Alice to perform measurements on her states, this question is important when one considers the idealized teleportation experiment that will be presented in Chapter 3. Levitons in an edge channel have to be distinguished from the underlying Fermi sea, which is not trivial to do. Electrons generated by the SAW technique travel in depleted channels, and the effect of the Fermi sea is removed, making it possible to detect these electrons. It has been suggested that electrons traveling in edge channels could be detected by having them interact with a nearby double quantum dot, although single-shot detection has not been achived yet [16, 26].

2.5 Scattering theory

Scattering theory is an important topic in physics. It has been used to study topics ranging from how celestial objects scatter in gravitational fields to how elementary particles interact with each other, and can be formulated both in terms of classical mechanics, relativity, and quantum mechanics [27, 28]. The idea is that you shoot particles into a region where they are subject to some type of interaction and study how their properties have changed as they leave the interaction region. In experiments, this might be done to

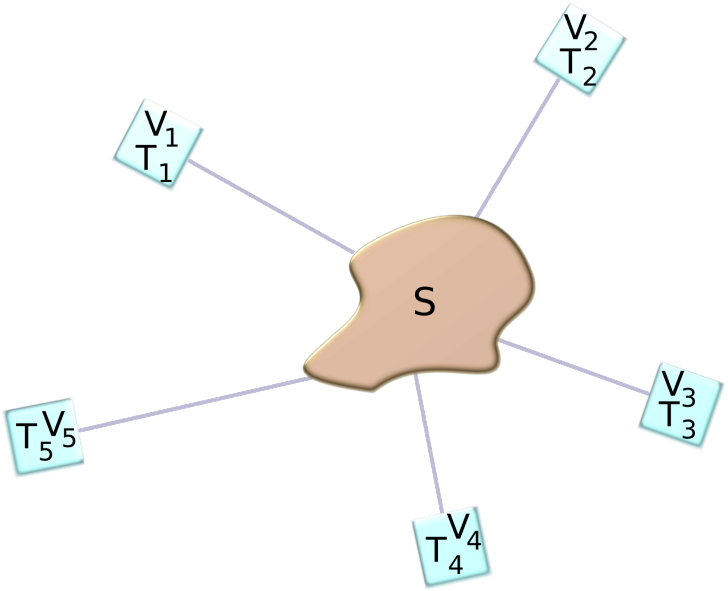

Figure 2.3: Illustration of a setup for a scattering experiment. Metallic contacts are connected to the scattering region S by one-dimensional leads. It is assumed that the temperature of the contacts are fixed and that we can control the voltage biases between them.

gain more knowledge of the scattering region itself, i.e. how a certain potential looks. An illustration of how a scattering experiment could look is shown in Figure 2.3. The perspective that will be used in this thesis is that scattering theory is useful in the calculation of transport properties of mesoscopic and nanoscale samples. If it is known how a single electron scatters, this should give a fairly good picture of how an electric current flows through the sample [29], provided electron-electron interactions are not too strong. One of the primary tools in the study of scattering in quantum mechanics is the scattering matrix, which relates the incoming states to the outgoing states.

2.5.1 Scattering matrix

This approach to scattering theory is built on using a scattering matrix to connect incoming and outgoing electron states. This is conveniently formulated within the second quantization framework, where the relevant objects are single-particle creation and annihilation operators defined by their action on states in the occupation number basis, i.e. where we represent a many-particle state by the number of particles that occupy each available mode. The annihilation operator a_i acting in the subspace corresponding to mode i annihilates the state where the mode is unoccupied

$$a_i \left|0\right\rangle_i = 0, \tag{2.28}$$

while the creation operator $a_i^\dagger$ acting on the same state will add a particle to that mode

$$a_i^\dagger \left|0\right\rangle_i = \left|1\right\rangle_i . \tag{2.29}$$

The creation and annihilation operators for electron states satisfy the fermionic anticommutation relations

$$\left\{a_i, a_j^\dagger\right\} = \delta_{ij}, \quad \{a_i, a_j\} = \left\{a_i^\dagger, a_j^\dagger\right\} = 0. \tag{2.30}$$

These anticommutation relations imply that each mode can only support one particle, since $a_i^\dagger a_i^\dagger = 0$, which is the Pauli exclusion principle. The scattering matrix relates the creation operators for incoming electrons a_j to the annihilation operators b_i for electrons leaving the scattering region by

$$b_i = \sum_j S_{ij} a_j. \tag{2.31}$$

A more formal discussion of this relation is provided in Section 2.5.2. The scattering matrix is required to be unitary since the scattering process should conserve probability. From Eq. (2.31) the creation operators of incoming and outgoing electrons are related by

$$b_i^\dagger = \sum_j S_{ij}^* a_j^\dagger. \tag{2.32}$$

The formalism presented so far will be enough for the calculations for teleportation performed under the assumption that single-electron detection is possible, since that calculation will simply rely on creating one electron at each of the source contacts and letting them scatter through the beamsplitters to the detector regions. When the periodic driving voltage is added, the picture changes since the Hamiltonian of the system will be time dependent and the sources are not creating just a single free electron but an electron wavepacket known as a leviton, which will be discussed in Section 2.6.

2.5.2 Floquet scattering theory

Floquet scattering theory is a way to treat scattering problems where the Hamiltonian is periodic in time. The general idea is that for such a system the single-particle wave functions can be written as [19, 30]

$$\Psi(t, \vec{r}) = e^{-i\frac{Et}{\hbar}} \phi(t, \vec{r}), \tag{2.33}$$

with energy E and ϕ a function periodic in t with the same period, $\mathcal{T}$, as the Hamiltonian. Expanding ϕ in a Fourier series gives

$$\Psi(t, \vec{r}) = e^{-i\frac{Et}{\hbar}} \sum_{q=-\infty}^{\infty} e^{-iq\Omega t} \psi_q(\vec{r}), \tag{2.34}$$

with $\Omega = 2\pi/\mathcal{T}$. If the time dependence of the Hamiltonian is due to the presence of a scattering potential of limited range, then far away from the scattering region the wavefunctions should look like plane waves, or Bloch waves if we are considering a crystal.

From Eq. (2.34) we can see that E is not well-defined, since one can make the transformation $E \to E + n\hbar\Omega$ and still recover the original Ψ by a simultaneous relabeling of the functions ψ_q by $\psi_q \to \psi_{q+n}$ [19, 30]. This will be given the interpretation that an electron with energy E entering the region of a scatterer with periodically time varying properties, can scatter into an outgoing state with energy $E + n\hbar\Omega$ where n is an integer. The scattering matrix that connects such states will be called the Floquet scattering matrix $S_F(E_n, E)_{\alpha\beta}$.

The system will be modeled as set of metallic contacts α, with temperature T_α and voltage V_α, connected to the scattering region by leads. The wavefunctions for electrons in the lead connected to contact α going into (out of) the scattering region are found by solving the Schrödinger equation. Close to the scatter, these functions may have

complicated shapes, but far away from the scatterer, they will look like sums of plane (Bloch) waves [31]. We choose boundary conditions such that the part of the wavefunction that looks like a plane wave or a Bloch wave entering (leaving) the scattering region from contact α has unit flux [19]. It is assumed that there is no backscattering at the interface between the contact and the lead, or in other words that scattering only takes place in the region marked S in Figure 2.3. The resulting wavefunctions will be the sum of the incoming (outgoing) parts, specified by the boundary conditions, and outgoing (incoming) parts that are a result of the presence of the scatterer. The Floquet scattering matrix will connect the incoming and outgoing states through the relation [32]

$$\Psi_\alpha^{\text{out}}(E) = \sum_{\beta,n} S_F(E,E_n)_{\alpha\beta}\Psi_\alpha^{\text{in}}(E_n), \qquad \Psi_\alpha^{\text{in}}(E) = \sum_{\beta,n} S_F^*(E_n,E)_{\beta\alpha}\Psi_\alpha^{\text{out}}(E_n), \tag{2.35}$$

where $\Psi_\alpha^{\text{in}}(E)$ and $\Psi_\alpha^{\text{out}}(E)$ are the incoming and outgoing states described above. Let the operators that annihilate these states be $a_\alpha(E)$, for the incoming, and $b_\alpha(E)$, for the outgoing. These operators also satisfy the relations in Eq. (2.35)

$$b_\alpha(E) = \sum_{\beta,n} S_F(E,E_n)_{\alpha\beta}a_\alpha(E_n), \qquad a_\alpha(E) = \sum_{\beta,n} S_F^*(E_n,E)_{\beta\alpha}b_\alpha(E_n). \tag{2.36}$$

The system that will be considered in this thesis will have no time dependence in the beamsplitters and phases, instead the time dependence is fully in the source contacts where the driving voltage is applied. This leads to a simplification in the form of the Floquet scattering matrix in that the individual elements can be written as the product of the Fourier coefficient of the phase that is picked up by the electrons leaving the contact and an element of the regular scattering matrix that describes the system when the time dependent voltages are removed. This factorization turns out to be very useful when computing the observables of interest since it allows one to separately deal with the sums over the Fourier indices and the channel indices.

Under the assumption that the potential in the contact is uniform, the electron wave functions in contact α pick up a time dependent phase factor $e^{i\phi_\alpha(t)}$ with

$$\phi_\alpha(t) = -\frac{1}{\hbar}\int_{-\infty}^{t} \mathrm{d}t' e V_\alpha(t'), \tag{2.37}$$

where $V_\alpha(t)$ is the voltage applied to contact α [19]. We then assume that there is no voltage in the leads that connect the contacts to the scattering region. With this assumption we can write the operators annihilating electron states leaving the contact with energy E in terms of the annihilation operators in the contacts as

$$a'_\alpha(E) = \sum_{n=\infty}^{\infty} S_\alpha(n)a_\alpha(E-n\hbar\Omega), \tag{2.38}$$

where

$$S_\alpha(n) = \frac{1}{\mathcal{T}}\int_0^{\mathcal{T}} e^{in\Omega t}e^{i\phi_\alpha(t)}, \tag{2.39}$$

are the Fourier coefficients of the phase that the electrons pick up in the contact [19].

Since the beamsplitters and phase differences are not time dependent, it is possible to connect the state leaving the scattering region towards contact α, $b_\alpha(E)$, to those entering the region, $a'_\beta(E)$, with a stationary scattering matrix as in the previous section

$$b_\alpha(E) = \sum_\beta S_{\alpha\beta}a'_\beta(E), \tag{2.40}$$

where it has also been assumed that the scattering is energy independent. In principle the beamsplitter transmission and reflection probabilities will depend on energy [33], but here we assume that this variation is small over the span of energies we are interested in, which are close to the Fermi energy. Using Eq. (2.38) in the previous equation gives

$$b_\alpha(E) = \sum_\beta \sum_{n=-\infty}^{\infty} S_{\alpha\beta} S_\beta(n) a_\beta(E - n\hbar\Omega) = \sum_\beta \sum_{n=-\infty}^{\infty} S_F(E, E_{-n})_{\alpha\beta} a_\beta(E_{-n}). \tag{2.41}$$

In the last equality the Floquet scattering matrix has been introduced. It connects states with energy $E_{-n} = E - n\hbar\Omega$ in contact β to outgoing states with energy E in lead α and in this case it takes the form

$$S_F(E, E_{-n})_{\alpha\beta} = S_{\alpha\beta} S_\beta(n). \tag{2.42}$$

Next we want to study how to compute observable quantities using Floquet theory, and we will start with the current operator in lead α. Under the assumption that only states close to the Fermi energy contribute significantly to the current, which is where there can be appreciable differences in two Fermi distributions, it can be reduced to [19]

$$\hat{I}_\alpha(t) = \frac{e}{h} \int\int \mathrm{d}E \mathrm{d}E' e^{i\frac{E-E'}{\hbar}t} \left[b_\alpha^\dagger(E) b_\alpha(E') - a_\alpha^\dagger(E) a_\alpha(E') \right], \tag{2.43}$$

where e represents the electron charge and a hat is used for the current operator to distinguish it from the average current. The expression for the current operator has a very intuitive form, since it says that the current in each lead is proportional to the difference between the number of states leaving and entering the scattering region. The Fourier transform of Eq. (2.43) gives

$$\hat{I}_\alpha(\omega) = e \int_{-\infty}^{\infty} \mathrm{d}E \left[b_\alpha^\dagger(E) b_\alpha(E + \hbar\omega) - a_\alpha^\dagger(E) a_\alpha(E + \hbar\omega) \right]. \tag{2.44}$$

For the purposes of this thesis, the current operator itself is not what is important but rather its quantum statistical average $I_\alpha(\omega) = \left\langle \hat{I}_\alpha(\omega) \right\rangle$. Under the assumption that the electrons in each contact are in thermal equilibrium and that electrons from different contacts are uncorrelated it is possible to calculate $I_\alpha(\omega)$ from the quantum statistical averages

$$\begin{aligned} \langle a_\alpha^\dagger(E) a_\beta(E') \rangle &= \delta_{\alpha\beta} \delta(E - E') f_\alpha(E), \\ \langle a_\alpha(E) a_\beta^\dagger(E') \rangle &= \delta_{\alpha\beta} \delta(E - E') \left(1 - f_\alpha(E)\right). \end{aligned} \tag{2.45}$$

Here

$$f_\alpha(E) = \frac{1}{e^{\frac{E-\mu_\alpha}{kT}} + 1}, \tag{2.46}$$

is the Fermi distribution in contact α and $\delta(E)$ is the Dirac delta distribution. For the case that we are interested in, $\mu_\alpha = 0$ for all α which means that there is no constant bias between any of the contacts. With the help of Eqs. (2.41) and (2.45) the average current can be expressed in terms of the Floquet scattering matrix and the Fermi distribution. The end result is

$$I(\omega) = \sum_{l=-\infty}^{\infty} 2\pi\delta(l\Omega - \omega) I_{\alpha,l}, \tag{2.47}$$

with

$$I_{\alpha,l} = \frac{e}{h}\int_{-\infty}^{\infty} \mathrm{d}E \left[\sum_{\beta}\sum_{n=-\infty}^{\infty} S_F^*(E,E_n)_{\alpha\beta} S_F(E_l,E_n)_{\alpha\beta} f(E_n) - \delta_{l0} f(E)\right]. \tag{2.48}$$

Computing the inverse Fourier transform of $I_\alpha(\omega)$ reveals that

$$I_\alpha(t) = \left\langle \hat{I}_\alpha(t) \right\rangle = \sum_{l=-\infty}^{\infty} e^{-il\Omega t} I_{\alpha,l}, \tag{2.49}$$

i.e. the $I_{\alpha,l}$ should be regarded as the Fourier components of $I_\alpha(t)$, which will be periodic with period $\mathcal{T}$. Here we will only concern ourselves with the direct current $I_{\alpha,0} = I_\alpha$ which corresponds to the average value of $I(t)$ over one period,

$$I_\alpha = \frac{1}{\mathcal{T}}\int_0^{\mathcal{T}} \mathrm{d}t I(t). \tag{2.50}$$

In addition to computing currents $I_\alpha(t)$ and current spectra $I_\alpha(\omega)$, Floquet scattering theory can be used to calculate correlation functions of different combinations of current operators, with the prototypical example being

$$P_{\alpha\beta}(t_1,t_2) = \left\langle \Delta\hat{I}_\alpha(t_1)\Delta\hat{I}_\beta(t_2)\right\rangle. \tag{2.51}$$

Here the current fluctuation operators $\Delta\hat{I}(t) = \hat{I}(t) - \left\langle \hat{I}(t)\right\rangle$ have been introduced. $P_{\alpha\beta}(t_1,t_2)$ is often defined in a symmetrized form, see e.g. ref. [19]. However, only correlators with $\alpha \neq \beta$ will be considered in this thesis. In that case $\hat{I}_\alpha(t_1)$ and $\hat{I}_\beta(t_2)$ commute, which can be checked using Eqs. (2.30) and (2.43), and the two definitions agree. The Fourier transform of Eq. (2.51) is

$$P_{\alpha\beta}(\omega_1,\omega_2) = \left\langle \Delta\hat{I}_\alpha(\omega_1)\Delta\hat{I}_\beta(\omega_2)\right\rangle. \tag{2.52}$$

Equation (2.52) will contain averages of products of four creation and annihilation operators, and each such product can be written as a sum of products of pairs of averages by an application of Wick's theorem, which also generalizes to larger products [34]. After applying Wick's theorem, Eqs. (2.41) and (2.45) can be used to show that

$$P_{\alpha\beta}(\omega_1,\omega_2) = \sum_{l=-\infty}^{\infty} 2\pi\delta(l\Omega - \omega_1 - \omega_2)\mathcal{P}_{\alpha\beta,l}(\omega_1,\omega_2), \tag{2.53}$$

where the $\mathcal{P}_{\alpha\beta,l}(\omega_1,\omega_2)$ are known as spectral noise powers. Again, the higher order l terms in the sum will not be of interest, and the relevant quantities will be the zero frequency correlators

$$\mathcal{P}_{\alpha\beta} = \mathcal{P}_{\alpha\beta,0}(0,0) = \int_0^{\mathcal{T}} \frac{\mathrm{d}t}{\mathcal{T}} \int_{-\infty}^{\infty} \mathrm{d}\tau P_{\alpha\beta}(t,t+\tau), \tag{2.54}$$

where the last equality can be proved by writing $P_{\alpha\beta}(t,t+\tau)$ as the Fourier transform of $P_{\alpha\beta}(\omega_1,\omega_2)$ and using Eq. (2.53).

The $\mathcal{P}_{\alpha\beta}$ is interpreted as the noise in the current due to fluctuations and can be written as the sum of two contributions, the thermal noise, $\mathcal{P}^{\rm th}_{\alpha\beta}$, and the shot noise, $\mathcal{P}^{\rm sh}_{\alpha\beta}$. Assuming that the Fermi distributions are the same in each contact, which will be true in the teleportation setup, the thermal noise takes the form

$$\begin{aligned}\mathcal{P}^{\rm th}_{\alpha\beta} = \frac{e^2}{h}\int_{-\infty}^{\infty} {\rm d}E f(E)\left(1-f(E)\right)\Bigg[\delta_{\alpha\beta}\Bigg(1+\sum_{\gamma}\sum_{n=-\infty}^{\infty}|S_F(E_n,E)_{\alpha\gamma}|^2\Bigg) \\ -\sum_{n=-\infty}^{\infty}\left(|S_F(E_n,E)_{\alpha\beta}|^2+|S_F(E_n,E)_{\beta\alpha}|^2\right)\Bigg],\end{aligned} \tag{2.55}$$

and the shot noise

$$\begin{aligned}\mathcal{P}^{\rm sh}_{\alpha\beta} = \frac{e^2}{2h}\int_{-\infty}^{\infty}{\rm d}E\sum_{\gamma\delta}\sum_{n,m,p=-\infty}^{\infty}\left(f(E_n)-f(E_m)\right)^2 S_F^*(E,E_n)_{\alpha\gamma}S_F(E_p,E_n)_{\beta\gamma} \\ \times S_F(E,E_m)_{\alpha\delta}S_F^*(E_p,E_m)_{\beta\delta}.\end{aligned} \tag{2.56}$$

$\mathcal{P}^{\rm th}_{\alpha\beta}$ will vanish at zero temperature due to the $f(E)(1-f(E))$ factor, and is therefore interpreted as arising from thermal fluctuations in the energy of the electrons, which are not present when $T=0$. $\mathcal{P}^{\rm sh}_{\alpha\beta}$ on the other hand can be nonzero also when $T=0$, but it will vanish if the scattering process is energy conserving, since then $S_F(E,E_n)_{\alpha\beta}\propto\delta_{n0}$, although this is a particular feature of assuming equal Fermi distributions in all contacts and it will be present if there are temperature or voltage differences between the contacts. The shot noise is usually interpreted as a consequence of the discrete nature of the electrons causing instantaneous current fluctuations in each contact [19]. Since the scattering is probabilistic, it will sometimes happen that more electrons end up at one contact and fewer at another which will cause a shift in the instantaneous values of the currents.

Below, we will also need to consider the third order correlator

$$Q_{\alpha\beta\gamma}(t_1,t_2,t_3)=\left\langle\Delta\hat{I}_\alpha(t_1)\Delta\hat{I}_\beta(t_2)\Delta\hat{I}_\gamma(t_3)\right\rangle, \tag{2.57}$$

and its Fourier transform

$$Q_{\alpha\beta\gamma}(\omega_1,\omega_2,\omega_3)=\left\langle\Delta\hat{I}_\alpha(\omega_1)\Delta\hat{I}_\beta(\omega_2)\Delta\hat{I}_\gamma(\omega_3)\right\rangle. \tag{2.58}$$

The argument that follows Eq. (2.51) concerning symmetrization also applies here. The same reasoning that lead to Eq. (2.53) can also be used to write $Q_{\alpha\beta\gamma}(\omega_1,\omega_2,\omega_3)$ as

$$Q_{\alpha\beta\gamma}(\omega_1,\omega_2,\omega_3)=\sum_{l=-\infty}^{\infty}2\pi\delta(l\Omega-\omega_1-\omega_2-\omega_3)\mathcal{Q}_{\alpha\beta\gamma,l}(\omega_1,\omega_2,\omega_3). \tag{2.59}$$

Again, we will only consider the zero frequency component

$$\mathcal{Q}_{\alpha\beta\gamma}=\mathcal{Q}_{\alpha\beta\gamma,0}(0,0,0)=\frac{1}{\mathcal{T}}\int_0^{\mathcal{T}}{\rm d}t\int_{-\infty}^{\infty}{\rm d}\tau_\beta\int_{-\infty}^{\infty}{\rm d}\tau_\gamma Q_{\alpha\beta\gamma}(t,t+\tau_\beta,t+\tau_\gamma). \tag{2.60}$$

2.6 Levitons

It has been shown that applying voltage pulses of Lorentzian shape in time to metallic contacts creates a quasiparticle excitation above the Fermi sea that consists of one electron

and no holes [35, 36]. These quasiparticles are called levitons. In this thesis levitons will be important when we consider the periodically driven teleportation setup, since the voltage pulses that are used are Lorentzian and will create levitons. It will be possible to interpret the measurement results as due to teleportation of leviton states. Levitons are named in the pioneering experimental work [37], after L. S. Levitov, who was one of people who theorized their existence [35, 36].

The voltage pulses that are used to create Levitons have the form

$$eV(t) = \sum_{j=-\infty}^{\infty} \frac{2\hbar\Gamma}{(t - j\mathcal{T})^2 + \Gamma^2}, \tag{2.61}$$

where $\mathcal{T}$ is the period of the pulse train and Γ is the width of each pulse. If such a voltage is applied to a contact in a scattering setup, then $S_\alpha(n)$ can be shown to take the form [18]

$$S_\alpha(n) = S(n) = \begin{cases} -2e^{-n\Omega\Gamma}\sinh(\Omega\Gamma) & n > 0 \\ e^{-\Omega\Gamma} & n = 0 \\ 0 & n < 0. \end{cases} \tag{2.62}$$

So an electron leaving the contact can keep its original energy or increase it by $n\hbar\Omega$, $n > 0$, but never decrease it since $S(n) = 0$ for $n < 0$. This has the interpretation that the voltage pulses create only electronic excitations and that no holes will be present. Note that for smaller Γ, higher energies will be involved.

The excitations that are created by the voltage pulses are called levitons and can be described by the following annihilation operator [36]

$$A_\alpha = \sqrt{2\Gamma} \sum_{E>0} e^{(it_\alpha - \Gamma)E/\hbar} a_\alpha(E), \tag{2.63}$$

where t_α is the time at which the leviton is created. At zero temperature, the voltage pulses will create a leviton each period. At finite temperature the created state will be a mixed one, and the simple interpretation of our results will no longer apply due to the presence of thermal excitations [38]. The energy distribution of the leviton wavepacket has an exponential shape above the Fermi energy, which means that the levitons can be thought of as having energy very close to the Fermi energy for large $\Gamma\Omega$. Since there are no holes accompanying the leviton, there will be no unoccupied states in the Fermi sea and the leviton is therefore very robust against energy relaxtion processes, meaning that relatively long coherence lengths should be possible when compared to other sources [16]. The spatial shape of the modulus squared of the leviton wavepacket will be a Lorentzian of width Γ [36] and this parameter is referred to when the width of levitons are discussed throughout the text.

Chapter 3

The teleportation setup

In this chapter the teleportation setup that has been studied in this thesis is presented and described. The first step is an abstract picture of the setup that can in principle be used to describe any implementation that uses backscattering free states. This will be followed by a more concrete realization of the setup, which is based on the Corbino disk geometry which is a 2DEG in the shape of an annulus. The Corbino geometry presented here can be used to realize the experiments that have been discussed in this thesis.

3.1 Teleporting a single electron

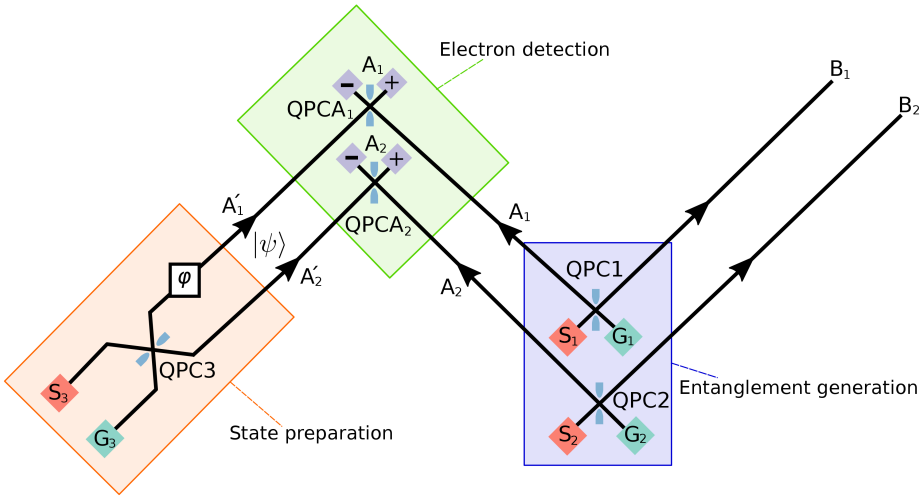

Figure 3.1: Schematic view of the teleportation setup. The S_i are single-electron sources, the G_i are grounded contacts, the QPCs act as beamsplitters. The A and A′ modes go to Alice while the B modes go to Bob. Electrons are detected at two detectors at A_1 and two detectors at A_2. The aim of the experiment is to transfer a superposition of A′ modes to a superposition of B modes.

The experiment that we want to describe is presented in Figure 3.1, which shows how the different components of the experimental setup are arranged. The architecture uses dual-rail qubits, where there are two spatial modes that an electron can occupy. We use as basis for our qubit space the states where one of the modes is occupied and the other is empty.

The first step is to prepare both the state that is going to be teleported, call it $|\psi\rangle$, and the shared entangled states. First, each of the three electron sources S_i generates an electron, which will travel towards the first set of beamsplitters, QPC1-QPC3. This can be described by the state

$$|\phi\rangle = a^\dagger_{S_3} a^\dagger_{S_1} a^\dagger_{S_2} |0\rangle . \tag{3.1}$$

The electron sources can for instance be one of the ones mentioned in Section 2.4.1, and since we will later work specifically with levitions, it can be useful to think of the sources as leviton sources. The scattering through QPC1 and QPC2 is described by the scattering matrix

$$S_j = \frac{1}{\sqrt{2}} \begin{bmatrix} i & 1 \\ 1 & i \end{bmatrix}, \tag{3.2}$$

while for QPC3 the scattering matrix is

$$S_3 = \begin{bmatrix} i\sqrt{R} & \sqrt{D} \\ \sqrt{D} & i\sqrt{R} \end{bmatrix}, \tag{3.3}$$

where R is the reflection probability and D the transmission probability, with $R + D = 1$. After QPC3 we also introduce a phase difference φ between the mode going to A_1 and the mode going to A_2. By using the scattering matrices for the QPC's and including φ, $|\phi\rangle$ can be expressed in terms of the A'_j, A_j and B_j modes as

$$\frac{1}{2}\left(i\sqrt{R}e^{-i\varphi}a^\dagger_{A'_1} + \sqrt{D}a^\dagger_{A'_2}\right)\left(ia^\dagger_{A_1} + a^\dagger_{B_1}\right)\left(ia^\dagger_{A_2} + a^\dagger_{B_2}\right)|0\rangle . \tag{3.4}$$

The A_1 and A_2 modes represent electrons traveling from the S_1 and S_2 sources, respectively, to Alice's detector regions. A'_1 and A'_2 modes instead represent electrons created at S_3 and heading to Alice. The B_1 and B_2 modes corresponds to electrons traveling to Bob. Each mode is labeled in Figure 3.1.

Equation (3.4) can be written as

$$|\psi\rangle |\Phi\rangle_1 |\Phi\rangle_2 , \tag{3.5}$$

with

$$|\psi\rangle = \left(i\sqrt{R}e^{-i\varphi}a^\dagger_{A'_1} + \sqrt{D}a^\dagger_{A'_2}\right)|0\rangle \tag{3.6}$$

and

$$|\Phi\rangle_j = \frac{1}{\sqrt{2}}\left(ia^\dagger_{A_j} + a^\dagger_{B_j}\right)|0\rangle . \tag{3.7}$$

If R, D and φ can be controlled then $|\psi\rangle$ can be any qubit state, and it is this superposition that we wish to teleport. $|\Phi\rangle_j$ is an entangled state since it has the form

$$\frac{1}{\sqrt{2}}\left(i\,|1\rangle_{A_j}|0\rangle_{B_j} + |0\rangle_{A_j}|1\rangle_{B_j}\right). \tag{3.8}$$

These are entangled single-particle states, as was mentioned in Section 2.4.3. It has been suggested that one can use entangled particle-hole pairs to teleport electrons [39], and there the entanglement is instead between two particles. We have so far prepared the state $|\psi\rangle$ that is going to be teleported, and we have generated entangled states that are shared between Alice and Bob.

Next, Alice performs her measurement. The first step of this procedure is to let the electron traveling to Alice pass through another set of Beamsplitters, $QPCA_1$ and

QPCA$_2$, that are also described by the scattering matrix S_j, defined in Eq. (3.2). Alice then measures the number of electrons in each mode $\mathrm{A}_j^{\pm}$. The state prior to Alice's measurement is

$$\begin{aligned}
&\frac{1}{2}\Bigg(\frac{1}{2}a^\dagger_{\mathrm{A}_1^+}a^\dagger_{\mathrm{A}_2^+}\left(i\sqrt{R}e^{-i\varphi}a^\dagger_{\mathrm{B}_1}+\sqrt{D}a^\dagger_{\mathrm{B}_2}\right)+\frac{1}{2}a^\dagger_{\mathrm{A}_1^-}a^\dagger_{\mathrm{A}_2^-}\left(i\sqrt{R}e^{-i\varphi}a^\dagger_{\mathrm{B}_1}+\sqrt{D}a^\dagger_{\mathrm{B}_2}\right)+\\
&+\frac{1}{2}a^\dagger_{\mathrm{A}_1^+}a^\dagger_{\mathrm{A}_2^-}\left(\sqrt{R}e^{-i\varphi}a^\dagger_{\mathrm{B}_1}+i\sqrt{D}a^\dagger_{\mathrm{B}_2}\right)-\frac{1}{2}a^\dagger_{\mathrm{A}_1^-}a^\dagger_{\mathrm{A}_2^+}\left(\sqrt{R}e^{-i\varphi}a^\dagger_{\mathrm{B}_1}+i\sqrt{D}a^\dagger_{\mathrm{B}_2}\right)+\\
&-\frac{i\sqrt{R}e^{-i\varphi}}{\sqrt{2}}\left(ia^\dagger_{\mathrm{A}_1^+}a^\dagger_{\mathrm{A}_1^-}a^\dagger_{\mathrm{A}_2^+}+a^\dagger_{\mathrm{A}_1^+}a^\dagger_{\mathrm{A}_1^-}a^\dagger_{\mathrm{A}_2^-}\right)+\frac{\sqrt{D}}{\sqrt{2}}\left(ia^\dagger_{\mathrm{A}_1^+}a^\dagger_{\mathrm{A}_2^+}a^\dagger_{\mathrm{A}_2^-}+a^\dagger_{\mathrm{A}_1^-}a^\dagger_{\mathrm{A}_2^+}a^\dagger_{\mathrm{A}_2^-}\right)-\\
&-\sqrt{R}e^{-i\varphi}a^\dagger_{\mathrm{A}_1^+}a^\dagger_{\mathrm{A}_1^-}a^\dagger_{\mathrm{B}_2}-i\sqrt{D}a^\dagger_{\mathrm{A}_2^+}a^\dagger_{\mathrm{A}_2^-}a^\dagger_{\mathrm{B}_1}+\\
&+\frac{1}{\sqrt{2}}\Big(i\sqrt{R}e^{-i\varphi}\left(a^\dagger_{\mathrm{A}_1^+}+ia^\dagger_{\mathrm{A}_1^-}\right)+\sqrt{D}\left(a^\dagger_{\mathrm{A}_2^+}+ia^\dagger_{\mathrm{A}_2^-}\right)\Big)a^\dagger_{\mathrm{B}_1}a^\dagger_{\mathrm{B}_2}\Bigg)|0\rangle=|\phi\rangle\,.
\end{aligned}\tag{3.9}$$

In terms of the B_1 and B_2 modes, the first four terms of $|\phi\rangle$ have a similar structure to $|\psi\rangle$. If one mode at each of A_1 and A_2 is occupied, then Bob's part of the state will be a superposition of his two modes. The rest of the terms in $|\phi\rangle$ do not have this structure. Some terms correspond to having all particles at Alice's location, which defeats the purpose of trying to send a state to Bob. Others have two particles at the same A_j, which means that Bob can not have a superposition of his two modes. In the remaining cases Bob ends up with two of the particles, which means that both of Bob's modes will be occupied, and he can therefore not have a superposition state. If Bob ends up with two particles, he has also lost his entanglement link to Alice. From this discussion we can conclude that our focus should be on outcomes where Alice finds one particle at A_1 and one at A_2, if we want to be able to teleport $|\psi\rangle$ to Bob. Analysis of the measurement outcomes and Bob's post-measurement state is performed in Section 4.1.

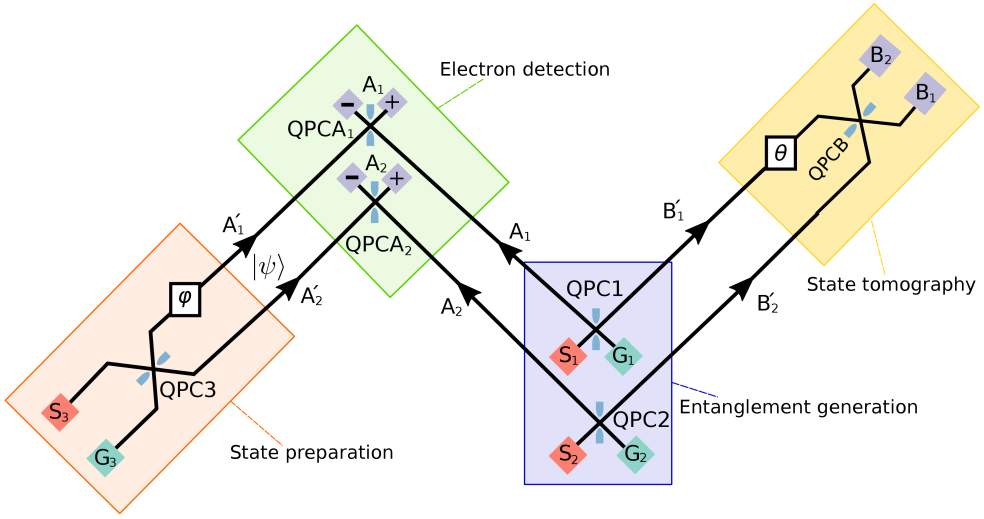

Figure 3.2: It is possible to compare Bob's state to the input state by estimating the components of the Bloch vector. For single-electron teleporation this can be done by measuring the difference in occupation number between Bob's two modes. Which component of the Bloch vector that is being measured can be selected by changing θ and the transparency of the beamsplitter QPCB.

In order to verify that the teleportation protocol is working, Bob can perform quantum state tomography on his part of the combined state. Quantum state tomography is a

way to estimate the state of a quantum system and it is based on the Bloch sphere representation of qubits presented in Section 2.2. From the results presented there, we know that by measuring the expectation value of σ_x, σ_y and σ_z on his state after Alice's measurement, Bob can estimate the Bloch vector $\vec{r'}$ of the state he received. Measuring $\langle\sigma_z\rangle$ for a qubit corresponds to a measurement of $\langle N_{\mathrm{B}_1} - N_{\mathrm{B}_2}\rangle$ in this case. $\langle\sigma_x\rangle$ and $\langle\sigma_y\rangle$ can also be expressed as $\langle N_{\mathrm{B}_1} - N_{\mathrm{B}_2}\rangle$, provided the state has been transformed appropriately prior to the measurement. To do this it suffices to apply a phase shift θ to one of the electron modes, and then let them pass through another beamsplitter, which we will call QPCB. The phase and the beamsplitter will implement the transformation

$$\begin{bmatrix} a^\dagger_{\mathrm{B}_1} \\ a^\dagger_{\mathrm{B}_2} \end{bmatrix} = \begin{bmatrix} \sqrt{D'}e^{i\theta} & i\sqrt{R'} \\ i\sqrt{R'}e^{i\theta} & \sqrt{D'} \end{bmatrix} \begin{bmatrix} a^\dagger_{\mathrm{B}'_1} \\ a^\dagger_{\mathrm{B}'_2} \end{bmatrix}, \tag{3.10}$$

where D' and R' are the transmission and reflection probabilities of the beamsplitter. A sketch of the tomography setup can be seen in Figure 3.2. The B′ modes are the modes going from the entanglement generation region to the state tomography region in Figure 3.2. The derivation of the correct settings for θ and QPCB is provided in Appendix A and the results are presented in Table 3.1.

Table 3.1: The phase and beamsplitter settings required for the different state tomography measurements.

Measurement	D'	θ
r'_x	$1/2$	$\pi/2$
r'_y	$1/2$	0
r'_z	1	0

The total scattering matrix for the entire system is found by combining the effect of scattering matrices for the individual QPCs. The result for our system is

$$\begin{bmatrix} a_{\mathrm{A}_1^+} \\ a_{\mathrm{A}_1^-} \\ a_{\mathrm{A}_2^+} \\ a_{\mathrm{A}_2^-} \\ a_{\mathrm{B}_1} \\ a_{\mathrm{B}_2} \end{bmatrix} = \frac{1}{\sqrt{2}} \begin{bmatrix} \frac{-1}{\sqrt{2}} & \frac{i}{\sqrt{2}} & 0 & 0 & i\sqrt{R}e^{-i\varphi} & \sqrt{D}e^{-i\varphi} \\ \frac{i}{\sqrt{2}} & \frac{1}{\sqrt{2}} & 0 & 0 & -\sqrt{R}e^{-i\varphi} & i\sqrt{D}e^{-i\varphi} \\ 0 & 0 & \frac{-1}{\sqrt{2}} & \frac{i}{\sqrt{2}} & \sqrt{D} & i\sqrt{R} \\ 0 & 0 & \frac{i}{\sqrt{2}} & \frac{1}{\sqrt{2}} & i\sqrt{D} & -\sqrt{R} \\ \sqrt{D'}e^{-i\theta} & i\sqrt{D'}e^{-i\theta} & -i\sqrt{R'} & \sqrt{R'} & 0 & 0 \\ -i\sqrt{R'}e^{-i\theta} & \sqrt{R'}e^{-i\theta} & \sqrt{D'} & i\sqrt{D'} & 0 & 0 \end{bmatrix} \begin{bmatrix} a_{\mathrm{S}_1} \\ a_{\mathrm{G}_1} \\ a_{\mathrm{S}_2} \\ a_{\mathrm{G}_2} \\ a_{\mathrm{S}_2} \\ a_{\mathrm{G}_3} \end{bmatrix}. \tag{3.11}$$

3.2 Periodically driven teleportation setup

Here we will consider what happens in the teleportation setup above when the sources are periodically injecting levitons into the experiment. This is a useful case to consider since the version presented above assumes that single-electron detection is possible, which is yet to be demonstrated for e.g. electrons in an edge channel, see Section 2.4.4. However, measurements of average currents and current cross correlators are possible to perform. Such quantities can be calculated using the machinery of Floquet scattering theory, which is presented in Section 2.5.2. One of the main results of this thesis is that it is possible

to relate the direct current, as well as second and third order cross correlators, to the quantities that are measured in the quantum state tomography part of the single-electron teleportation setup. There has been previous suggestions that state tomography can be performed on electrons by measuring current correlators [40]. The approach presented here uses the assumption that the leviton sources are configured so that the temporal width of each leviton is sufficiently small, meaning that levitons emitted during different periods are uncorrelated. If the period of the voltage is sufficiently long, we can say that only levitons emitted during the same period are passing through the setup at any one time, which recreates the picture of teleportation given in the previous section. We can interpret this as repeating the teleportation experiment very many times. Typical leviton sources operate at GHz frequencies [37].

3.3 Corbino disk experimental geometry

Before the situations that have been discussed so far are analyzed further, a more concrete experimental implementation of the experiment is presented. The setup is based on the Corbino disk geometry for the quantum Hall effect. A Corbino disk is an annular sample of a material that supports a 2DEG, and is brought into the integer QHE through the use of strong magnetic fields. The edge states propagate along the bounding circles. A Corbino disk can be thought of as a regular Hall bar that has been joined along the short edges. Figure 3.3 shows how the experiments described above can be mapped onto a Corbino setup. Similar setups have been studied before [41, 42], and it can be shown that currents and second order correlators do not depend on the phases, while third order correlators will depend on the sum of the phases, which can be tuned by altering a magnetic flux Φ that that is threaded through the center of the disk. The Corbino disk is named after O. M. Corbino, who studied magnetoresistance using an annular geometry [43, 44].

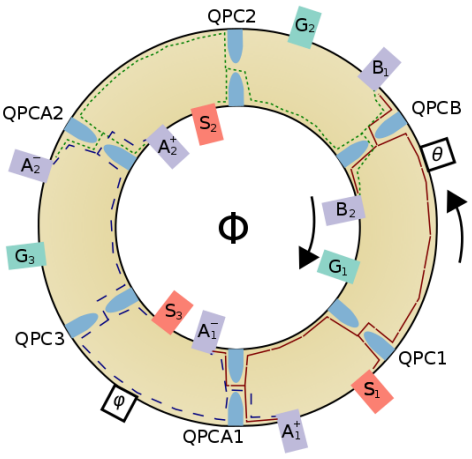

Figure 3.3: An illustration of a possible experimental setup, based on a Corbino disk. Electrons are generated at the sources (red) and travel along the boundaries of the disk, with the possible trajectories indicated by the lines. The two arrows indicate the direcetion of travel for the corresponding edge states. The QPCs (blue) act as beamsplitters and facilitate scattering between the two edges, with scattering matrices defined in Section 3.1. Phase differences φ and θ are introduced along two of the paths and their sum, which is what the observables of interest depend on, can be tuned by altering a magnetic flux Φ. Current measurements are performed at six different detectors (purple).

Chapter 4

Results

This chapter presents the results of the calculations that have been performed in this thesis. To start with, the focus will be on the single-electron picture of teleportation where it is assumed that single-electron detection is possible. After that the focus will be shifted to the results for the periodically driven teleportation setup, starting with what happens at zero temperature and then what changes when finite temperatures are introduced.

4.1 Single-electron picture

Here an analysis of Alice's measurement and Bob's post-measurement state is presented. First a POVM describing ideal single-electron detection will be defined. This will be followed by the results for the teleportation efficiency and the post-measurement states. Lastly, we will discuss the state tomography procedure in light of these results.

4.1.1 Basic picture and measurement

From the discussion following Eq. (3.9), we know that the measurement outcomes that are interesting for teleportation are those where two particles are detected at A with one at A_1 and the other at A_2. These leave one particle at B, and it can be in a superposition of the two B modes. If two particles are detected at A_1 for instance, then the third is found with complete certainty in the B_2 mode. If one takes the point of view that was presented in Section 2.1, then the useful outcomes are those where Alice cannot tell where the electron created at S_3 was detected, and that means she does not learn anything about the state $|\psi\rangle$ that we want to teleport. The useful outcomes can be labeled by $j_i \in \{+,-\}$, depending on which of the modes at A_i is occupied. Appendix B contains the definition of the full POVM for Alice's measurement. There it is also verified that the POVM fulfills the conditions specified in Section 2.3. The POVM elements $E(j_1, j_2)$ for the relevant outcomes are

$$\begin{aligned}
E(+,+) &= N_{A_1^+} N_{A_2^+} (I - N_{A_1^-})(I - N_{A_2^-}), \\
E(+,-) &= N_{A_1^+} N_{A_2^-} (I - N_{A_1^-})(I - N_{A_2^+}), \\
E(-,+) &= N_{A_1^-} N_{A_2^+} (I - N_{A_1^+})(I - N_{A_2^-}), \\
E(-,-) &= N_{A_1^-} N_{A_2^-} (I - N_{A_1^+})(I - N_{A_2^+}).
\end{aligned} \tag{4.1}$$

$N_k = a_k^\dagger a_k$ is the number operator for mode k. These operators project the state onto the subspace where the j_1 and j_2 modes are occupied. The probability for Alice to find each of the desired outcomes is $1/16$, as can be seen by calculating $p(+,+)$

$$\begin{aligned} p(+,+) &= \langle\phi| E(+,+) |\phi\rangle = \langle\phi| N_{\mathrm{A}_1^+} N_{\mathrm{A}_2^+} (I - N_{\mathrm{A}_1^-})(I - N_{\mathrm{A}_2^-}) |\phi\rangle = \\ &= \frac{1}{4} \langle\phi| a^\dagger_{A_1^+} a^\dagger_{A_2^+} \left(i\sqrt{R} a^\dagger_{\mathrm{B}_1} + \sqrt{D} a^\dagger_{\mathrm{B}_2} \right) |0\rangle = \frac{1}{16}. \end{aligned} \tag{4.2}$$

The calculations for the three other cases follow the exact same steps.

Since the interesting part of the post-measurement state is the state at B, it makes sense to study the partial trace over states at A of the post-measurement density matrix. As was shown in Section 2.3, it is not necessary to define Kraus operators for this measurement to find Bob's post-measurement state, since when calculating the partial trace it suffices to know the POVM elements. Calculating the post-measurement states for the four relevant measurement outcomes results in

$$\begin{aligned} \rho_B(+,+) &= \left(i\sqrt{R} e^{-i\varphi} a^\dagger_{\mathrm{B}_1} + \sqrt{D} a^\dagger_{\mathrm{B}_2} \right) |0\rangle \langle 0| \left(-i\sqrt{R} e^{i\varphi} a_{\mathrm{B}_1} + \sqrt{D} a_{\mathrm{B}_2} \right) = |\psi\rangle \langle\psi| , \\ \rho_B(-,-) &= \left(i\sqrt{R} e^{-i\varphi} a^\dagger_{\mathrm{B}_1} + \sqrt{D} a^\dagger_{\mathrm{B}_2} \right) |0\rangle \langle 0| \left(-i\sqrt{R} e^{i\varphi} a_{\mathrm{B}_1} + \sqrt{D} a_{\mathrm{B}_2} \right) = |\psi\rangle \langle\psi| , \\ \rho_B(+,-) &= \left(\sqrt{R} e^{-i\varphi} a^\dagger_{\mathrm{B}_1} + i\sqrt{D} a^\dagger_{\mathrm{B}_2} \right) |0\rangle \langle 0| \left(\sqrt{R} e^{i\varphi} a_{\mathrm{B}_1} - i\sqrt{D} a_{\mathrm{B}_2} \right) = U |\psi\rangle \langle\psi| U^\dagger, \\ \rho_B(-,+) &= \left(\sqrt{R} e^{-i\varphi} a^\dagger_{\mathrm{B}_1} + i\sqrt{D} a^\dagger_{\mathrm{B}_2} \right) |0\rangle \langle 0| \left(\sqrt{R} e^{i\varphi} a_{\mathrm{B}_1} - i\sqrt{D} a_{\mathrm{B}_2} \right) = U |\psi\rangle \langle\psi| U^\dagger, \end{aligned} \tag{4.3}$$

where U is the unitary transformation

$$U = \begin{bmatrix} -i & 0 \\ 0 & i \end{bmatrix} \tag{4.4}$$

on the space spanned by $a^\dagger_{\mathrm{B}_1} |0\rangle$ and $a^\dagger_{\mathrm{B}_2} |0\rangle$. The first two states are the same as the state we wished to teleport, and they are found with a total probability of $1/8$. The two following states can be transformed into the original state by applying $U^\dagger$, and they are also found with a total probability of $1/8$. This means that teleportation is successful $1/8$ or $1/4$ of the time, depending on whether it is possible to apply $U^\dagger$ to the state at B.

Compared to the original teleportation protocol [1], which in principle has a 100% success rate, our approach can only be successful 25% of the time. However, the original protocol has four different outcomes at B, whereas here there are only two outcomes at B when teleportation is successful. If the unitary transformation at B is not implemented in both of the protocols then the standard protocol is successful 25% of the time while our approach would be successful 12,5% of the time. We have now showed that it is in principle possible to perform (probabilistic) quantum teleportation using an electron quantum optics approach. Improving the efficiency figures, if possible, would require a change in architecture, presumably one that minimizes the number of outcomes that do not contribute to teleportation. Trying to scale probabilistic protocols to perform more complex quantum information processing tasks requires care, so that run time is not wasted by unwanted outcomes.

4.1.2 State tomography

For teleportation, the only interesting cases to perform state tomography on Bob's state are those where teleportation should have succeeded. This means that we should only

perform the tomography measurement when Alice has obtained an outcome where teleportation is possible. Assuming Alice got outcome X for her measurement, then Bob's post measurement state ρ_{B} is given by Eq. (2.25). Combining this with Eq. (2.26) tells us that the Bloch vector components of Bob's state, given that Alice gets outcome X, are

$$\begin{aligned} r_i' &= \mathrm{Tr}\left(\sigma_i \rho_B\right) = \frac{1}{P(X)} \mathrm{Tr}\left(I_A \otimes \sigma_i M\left(X\right) \rho M^\dagger\left(X\right)\right) = \frac{1}{P(X)} \mathrm{Tr}\left(E(X)\sigma_i \rho\right) = \\ &= \frac{1}{P(X)} \langle E(X)\sigma_i \rangle, \end{aligned} \tag{4.5}$$

where $\{M(X)\}$ is any set of Kraus operators that gives rise to the POVM defined in Eq. 4.1. Since our tomography setup always ensures that a measurement of $\langle \sigma_i \rangle$ corresponds to a measurement of $\langle N_{\mathrm{B}_1} - N_{\mathrm{B}_2} \rangle$ we can write

$$r_i' = \frac{1}{P(X)} \langle E(X)(N_{\mathrm{B}_1} - N_{\mathrm{B}_2}) \rangle, \tag{4.6}$$

with the appropriate values of D' and θ so that this corresponds to measuring the i component of the Bloch vector of Bob's state. Computing r_i for the state we wish to teleport gives

$$\begin{aligned} r_x &= 2\sqrt{RD}\sin\varphi, \\ r_y &= -2\sqrt{RD}\cos\varphi, \\ r_z &= R - D. \end{aligned} \tag{4.7}$$

This is also what one finds by computing r_i' for the teleported state with the method described above, if Alice measures $++$. This case is sufficient to consider in order to demonstrate that teleportation works, since we are not implementing the conditional unitary transformation that would mean that also the $+-$ and $-+$ outcomes could be used for teleportation. Equation (4.6) for the outcome $++$ becomes

$$r_i' = \frac{\langle E(1,0,1,0)(N_{\mathrm{B}_1} - N_{\mathrm{B}_2}) \rangle}{\langle E(1,0,1,0) \rangle} = \frac{\langle N_{\mathrm{A}_1^+} N_{\mathrm{A}_2^+} (N_{\mathrm{B}_1} - N_{\mathrm{B}_2}) \rangle}{\langle N_{\mathrm{A}_1^+} N_{\mathrm{A}_2^+} (I - N_{\mathrm{A}_1^-} + N_{\mathrm{A}_2^-}) \rangle}, \tag{4.8}$$

where in the last expression we have dropped terms that involve more than three electrons, since there are only three electrons in the system.

4.2 Periodic driving and levitons

We now present the results of having the teleportation setup driven by the voltage pulses that create levitons. The first step is to show how we can relate the state tomography measurements that were performed in the previous section to observables that can be calculated using Floquet scattering theory. These involve correlators up to order three. The final step will be to present the temperature dependence of the involved quantities, with special attention given to the case $T = 0$ where we can make a clear interpretation of the results as being due to quantum teleportation of levitons. When we go to finite temperatures, an interpretation in terms of single-particle teleportation becomes difficult due to the presence of other excitations, but we will see that the results can still be given the interpretation of average quantities describing noisy teleportation of a leviton.

4.2.1 Current correlators and the single-shot picture

In order to perform the state tomography described in Section 3.1 in the setup where we periodically inject levitons, we need to find observables that can be connected to Eq. (4.8). The goal of this section is to show that at zero temperature it is possible to find a correspondence between leviton number operators and current correlators. One example of such a correspondence is

$$\langle N_\alpha N_\beta N_\gamma\rangle = \frac{\mathcal{T}}{e^3}\mathcal{Q}_{\alpha\beta\gamma} + \frac{\mathcal{T}^2}{e^3}\left(I_\alpha\mathcal{P}_{\beta\gamma} + I_\beta\mathcal{P}_{\alpha\gamma} + I_\gamma\mathcal{P}_{\alpha\beta}\right) + \frac{\mathcal{T}^3}{e^3}I_\alpha I_\beta I_\gamma. \tag{4.9}$$

This is important because Eq. (4.8) implies that the Bloch vector of the teleported state, and the success probability, can be expressed in terms of different combinations of number operators. With this correspondence we will be able to express these quantities in terms of correlators, and therefore have another way to measure them.

As was discussed in Section 2.5.2, the quantities I_α, $\mathcal{P}_{\alpha\beta}$ and $\mathcal{Q}_{\alpha\beta\gamma}$ can be expressed in the following way

$$I_\alpha = \frac{1}{\mathcal{T}}\int_0^{\mathcal{T}} \mathrm{d}t\langle\hat{I}_\alpha(t)\rangle, \tag{4.10a}$$

$$\mathcal{P}_{\alpha\beta} = \frac{1}{\mathcal{T}}\int_0^{\mathcal{T}} \mathrm{d}t\int_{-\infty}^{\infty} \mathrm{d}\tau\langle\Delta\hat{I}_\alpha(t)\Delta\hat{I}_\beta(t+\tau)\rangle, \tag{4.10b}$$

$$\mathcal{Q}_{\alpha\beta\gamma} = \frac{1}{\mathcal{T}}\int_0^{\mathcal{T}} \mathrm{d}t\int_{-\infty}^{\infty} \mathrm{d}\tau_\beta\int_{-\infty}^{\infty} \mathrm{d}\tau_\gamma\langle\Delta\hat{I}_\alpha(t)\Delta\hat{I}_\beta(t+\tau_\beta)\Delta\hat{I}_\gamma(t+\tau_\gamma)\rangle. \tag{4.10c}$$

Since our system is periodic in time with period $\mathcal{T}$, we define the operator for the number of electrons detected in contact α during one period of the external voltage as

$$N_\alpha = \frac{1}{e}\int_0^{\mathcal{T}} \mathrm{d}t\hat{I}_\alpha(t). \tag{4.11}$$

Using Eq. (4.10a), the expectation value for N_α is seen to be

$$\langle N_\alpha\rangle = \frac{\mathcal{T}}{e}I_\alpha. \tag{4.12}$$

With $\Delta N_\alpha = N_\alpha - \langle N_\alpha\rangle$ we find

$$\langle\Delta N_\alpha\Delta N_\beta\rangle = \frac{1}{e^2}\int_0^{\mathcal{T}} \mathrm{d}t\int_0^{\mathcal{T}} \mathrm{d}\tau\langle\Delta\hat{I}_\alpha(t)\Delta\hat{I}_\beta(\tau)\rangle = \frac{\mathcal{T}}{e^2}\frac{1}{\mathcal{T}}\int_0^{\mathcal{T}} \mathrm{d}t\int_{-t}^{\mathcal{T}-t} \mathrm{d}\tau\langle\Delta\hat{I}_\alpha(t)\Delta\hat{I}_\beta(t+\tau)\rangle. \tag{4.13}$$

We now assume that $\Delta\hat{I}_\alpha(t)$ and $\Delta\hat{I}_\beta(t')$ are uncorrelated when t and t' lie in different periods, i.e. $\langle\Delta\hat{I}_\alpha(t)\Delta\hat{I}_\beta(t')\rangle = 0$ for $\lfloor t/\mathcal{T}\rfloor \neq \lfloor t'/\mathcal{T}\rfloor$, where $\lfloor x\rfloor$ is the floor function. This assumption is expected to be valid if the Lorentzian voltage pulses have small widths, such that subsequent pulses do not overlap significantly. From this we can show that

$$\mathcal{P}_{\alpha\beta} = \frac{1}{\mathcal{T}}\int_0^{\mathcal{T}} \mathrm{d}t\int_{\lfloor\frac{t}{\mathcal{T}}\rfloor=\lfloor\frac{t+\tau}{\mathcal{T}}\rfloor} \mathrm{d}\tau\langle\Delta\hat{I}_\alpha(t)\Delta\hat{I}_\beta(t+\tau)\rangle = \frac{1}{\mathcal{T}}\int_0^{\mathcal{T}} \mathrm{d}t\int_{-t}^{\mathcal{T}-t} \mathrm{d}\tau\langle\Delta\hat{I}_\alpha(t)\Delta\hat{I}_\beta(t+\tau)\rangle. \tag{4.14}$$

From Eqs. (4.13) and (4.14) it follows that

$$\langle\Delta N_\alpha\Delta N_\beta\rangle = \frac{\mathcal{T}}{e^2}\mathcal{P}_{\alpha\beta}. \tag{4.15}$$

For $\langle \Delta N_\alpha \Delta N_\beta \Delta N_\gamma \rangle$ we get

$$\begin{aligned}\langle \Delta N_\alpha \Delta N_\beta \Delta N_\gamma \rangle &= \frac{\mathcal{T}}{e^3}\frac{1}{\mathcal{T}}\int_0^{\mathcal{T}} \mathrm{d}t \int_0^{\mathcal{T}} \mathrm{d}\tau_\beta \int_0^{\mathcal{T}} \mathrm{d}\tau_\gamma \langle \Delta \hat{I}_\alpha(t)\Delta \hat{I}_\beta(\tau_\beta)\Delta \hat{I}_\gamma(\tau_\gamma)\rangle = \\ &= \frac{\mathcal{T}}{e^3}\frac{1}{\mathcal{T}}\int_0^{\mathcal{T}} \mathrm{d}t \int_{-t}^{\mathcal{T}-t} \mathrm{d}\tau_\beta \int_{-t}^{\mathcal{T}-t} \mathrm{d}\tau_\gamma \langle \Delta \hat{I}_\alpha(t)\Delta \hat{I}_\beta(t+\tau_\beta)\Delta \hat{I}_\gamma(t+\tau_\gamma)\rangle.\end{aligned} \tag{4.16}$$

Under the assumption that $\langle \Delta \hat{I}_\alpha(t)\Delta \hat{I}_\beta(t')\Delta \hat{I}_\gamma(t'')\rangle$ vanishes unless t, t' and t'' all lie in the same period, $\mathcal{Q}_{\alpha\beta\gamma}$ becomes

$$\begin{aligned}\mathcal{Q}_{\alpha\beta\gamma} &= \frac{1}{\mathcal{T}}\int_0^{\mathcal{T}} \mathrm{d}t \int_{-\infty}^{\infty} \mathrm{d}\tau_\beta \int_{-\infty}^{\infty} \mathrm{d}\tau_\gamma \langle \Delta \hat{I}_\alpha(t)\Delta \hat{I}_\beta(t+\tau_\beta)\Delta \hat{I}_\gamma(t+\tau_\gamma)\rangle = \\ &= \frac{1}{\mathcal{T}}\int_0^{\mathcal{T}} \mathrm{d}t \int_{-t}^{\mathcal{T}-t} \mathrm{d}\tau_\beta \int_{-t}^{\mathcal{T}-t} \mathrm{d}\tau_\gamma \langle \Delta \hat{I}_\alpha(t)\Delta \hat{I}_\beta(t+\tau_\beta)\Delta \hat{I}_\gamma(t+\tau_\gamma)\rangle.\end{aligned} \tag{4.17}$$

We therefore have

$$\langle \Delta N_\alpha \Delta N_\beta \Delta N_\gamma \rangle = \frac{\mathcal{T}}{e^3}\mathcal{Q}_{\alpha\beta\gamma}. \tag{4.18}$$

From the relation

$$\begin{aligned}\langle N_\alpha N_\beta N_\gamma \rangle = \langle N_\alpha\rangle\langle N_\beta\rangle\langle N_\gamma\rangle + \langle \Delta N_\alpha \Delta N_\beta\rangle\langle N_\gamma\rangle + \langle \Delta N_\alpha \Delta N_\gamma\rangle\langle N_\beta\rangle + \\ + \langle \Delta N_\beta \Delta N_\gamma\rangle\langle N_\alpha\rangle + \langle \Delta N_\beta \Delta N_\gamma \Delta N_\alpha\rangle,\end{aligned} \tag{4.19}$$

we can establish Eq. (4.9). Similar relations for e.g. $\langle N_\alpha N_\beta\rangle$ can be established analogously. The procedure used to find the correspondences could in principle be extended to higher order correlators. However, for the purposes of demonstrating teleportation with levitons, it suffices to consider correlators up to order three, since Eq. (4.8) does not contain higher orders.

4.2.2 Expressions for the Correlators

We will now turn to computing the relevant currents and current correlators. For the currents we use Eq. (2.44). Since our scattering matrix is of the form Eq. (2.42), we can write the current as

$$\begin{aligned}I_\alpha &= \frac{e}{h}\sum_\beta |S_{\alpha\beta}|^2 \sum_{n=-\infty}^{\infty} |S_\beta(-n)|^2 \int_{-\infty}^{\infty} \mathrm{d}E(f(E_n) - f(E)) = \\ &= \frac{e}{\mathcal{T}}\sum_{\beta=\mathrm{S}_i} |S_{\alpha\beta}|^2 \sum_{n=1}^{\infty} n\,|S(n)|^2 = \frac{e}{\mathcal{T}}\sum_{\beta=\mathrm{S}_i} |S_{\alpha\beta}|^2,\end{aligned} \tag{4.20}$$

where the notation $\sum_{\beta=\mathrm{S}_i}$ means that the sum runs only over source contacts. The second equality in Eq. (4.20) follows from the result $\int_{-\infty}^{\infty} \mathrm{d}E(f(E_n) - f(E)) = -n\hbar\Omega$, which can be seen by a straightforward computation, and the last equality is due to $\sum_{n=1}^{\infty} n\,|S(n)|^2 = 1$, which corresponds to the number of electrons emitted from each of the sources every period [45]. From Eq. (4.20) we can see that the direct currents in the teleportation setup are temperature independent. It also has a rather intuitive form, since it is the sum of the currents emitted by each source, weighted by the probability that an electron from source S_i will end up at contact α. (Each source emits one electron per period on average.)

Next we compute $\mathcal{P}_{\alpha\beta}$. This means evaluating the expressions (2.55) and (2.56) for the thermal and shot noise. The first term of the thermal noise can be seen to be zero for $\alpha \neq \beta$ and the second term vanishes in chiral systems when both α and β refer to detector contacts, since there are no scattering elements that connect them. Since these are exactly the types of correlators we are interested in for teleportation, we can disregard the thermal noise. We can then insert the expression for the scattering matrix into Eq. (2.56) which gives,

$$\mathcal{P}_{\alpha\beta} = \frac{e^2}{2h} \sum_{\gamma\delta} \sum_{n,m,p=-\infty}^{\infty} \chi(n-m) S^*_{\alpha\gamma} S_{\beta\gamma} S_{\alpha\delta} S^*_{\beta\delta} S^*_{\gamma}(-n) S_{\gamma}(p-n) S_{\delta}(-m) S^*_{\delta}(p-m). \tag{4.21}$$

The function $\chi(n-m)$ is defined as

$$\chi(n-m) = \int_{-\infty}^{\infty} \mathrm{d}E (f(E_n) - f(E_m))^2 = (n-m)\hbar\Omega \coth \frac{(n-m)\hbar\Omega}{2k_{\mathrm{B}}T} - 2k_{\mathrm{B}}T. \tag{4.22}$$

This expression can be simplified somewhat by evaluating the sums over n, m and p for the different combinations of γ and δ. A result that is helpful is a convolution theorem for Fourier coefficients of two periodic functions f and h, stated in ref. [19] as

$$\sum_{n=-\infty}^{\infty} \hat{f}(n) \left(\hat{h}(n+q)\right)^* = \widehat{fh^*}(-q), \tag{4.23}$$

where $\hat{f}(n)$ is the n-th Fourier coefficient of f etc. The sum in Eq. (4.21) contains many factors of the form $\sum_{n=-\infty}^{\infty} S(n)S^*(n+q)$ that reduce to δ_{q0} since $S(n)$ are the Fourier coefficients of a phase. If $f = h = e^{i\varphi}$, then $fh^* = 1$, which has δ_{q0} as its Fourier coefficients. The final result is

$$\mathcal{P}_{\alpha\beta} = \frac{e^2 F(T)}{2\mathcal{T}} \left(\sum_{\gamma=\mathrm{S}_i} \sum_{\delta=\mathrm{G}_i} + \sum_{\gamma=\mathrm{G}_i} \sum_{\delta=\mathrm{S}_i} \right) S^*_{\alpha\gamma} S_{\beta\gamma} S_{\alpha\delta} S^*_{\beta\delta} = F(T) \mathcal{P}_{\alpha\beta}\Big|_{T=0}, \tag{4.24}$$

where the sums run over source contacts S_i or grounded contacts G_i. The function $F(T)$ is defined as

$$F(T) = \sum_{n=1}^{\infty} n \left(\coth \frac{n\hbar\Omega}{2k_{\mathrm{B}}T} - 2\frac{k_{\mathrm{B}}T}{n\hbar\Omega} \right) |S(n)|^2 . \tag{4.25}$$

Equation (4.24) says that the noise is the product of two factors. One factor corresponds to the noise at zero temperature, and depends only on the details of the settings of the teleportation setup, which is encoded in the $S_{\alpha\beta}$. The other factor, $F(T)$, depends on the temperature and the settings of the leviton sources.

An expression for the third order correlator is derived in Appendix C. With the Floquet scattering matrix that describes our system it takes the form

$$\begin{aligned} \mathcal{Q}_{\alpha\beta\gamma} = \frac{e^3}{h} \sum_{\delta\varepsilon\zeta} \sum_{k,n,s,u,v=-\infty}^{\infty} & S^*_{\delta}(-n) S_{\delta}(k-v-n) S_{\varepsilon}(-s) S^*_{\varepsilon}(k-u-s) S_{\zeta}(-u) S^*_{\zeta}(-v) \\ & \left(M_{\delta\varepsilon\zeta} G(n-k, s-k) - M^*_{\delta\varepsilon\zeta} G(k-n, k-s) \right), \end{aligned} \tag{4.26}$$

with

$$M_{\delta\varepsilon\zeta} = S^*_{\alpha\delta} S_{\gamma\delta} S_{\alpha\varepsilon} S^*_{\beta\varepsilon} S_{\beta\zeta} S^*_{\gamma\zeta}. \tag{4.27}$$

The function $G(n-k, s-k)$, which is an energy integral over Fermi distributions, is defined in Appendix C. $G(n-k, s-k)$ can be evaluated analytically, with the result

$$G(n-k, s-k) = \frac{\hbar\Omega}{8} \frac{(n-s)e^{(k-n)\frac{\hbar\Omega}{k_\mathrm{B}T}} + (k-n)e^{(s-n)\frac{\hbar\Omega}{k_\mathrm{B}T}} + s - k}{\sinh\frac{(n-k)\hbar\Omega}{2k_\mathrm{B}T} \sinh\frac{(n-s)\hbar\Omega}{2k_\mathrm{B}T} \sinh\frac{(s-k)\hbar\Omega}{2k_\mathrm{B}T}}. \tag{4.28}$$

The five infinite sums in Eq. (4.26) can be reduced to single infinite sums by making use of Eq. (4.23). Calculating this for the possible combinations of detectors for the cross correlators shows that we will end up in a similar situation to that of the noise, in that we can separate $\mathcal{Q}_{\alpha\beta\gamma}$ into one factor that depends only on the beamsplitter and phase settings, and one that depends on the temperature and the source settings, i.e

$$\mathcal{Q}_{\alpha\beta\gamma} = A(T)\mathcal{Q}_{\alpha\beta\gamma}\Big|_{T=0}. \tag{4.29}$$

It also turns out that the temperature dependent factor $A(T)$ takes the same form for every detector combination, namely

$$A(T) = \sum_{n=1}^{\infty} n \left(\coth^2 \frac{n\hbar\Omega}{2k_\mathrm{B}T} + \frac{1}{2}\operatorname{csch}^2 \frac{n\hbar\Omega}{2k_\mathrm{B}T} - 3\frac{k_\mathrm{B}T}{n\hbar\Omega}\coth\frac{n\hbar\Omega}{2k_\mathrm{B}T} \right) |S(n)|^2 . \tag{4.30}$$

From the definitions of r'_i in terms of POVM elements discussed in Section 4.1.2 and from the correspondence derived in the previous section, we see that the currents and correlators that are relevant for demonstrating teleportation are those listed in Table 4.1. The table contains their values at zero temperature and their temperature dependence. Like in Section 4.1.2, we focus on the case when Alice measures $++$.

Table 4.1: Expressions for the currents and correlators that are needed to demonstrate teleportation. The expressions are given for the three different tomography measurements needed to determine the state at B, and those expressions are valid at $T = 0$. The last column gives the temperature dependent factors of each quantity.

Quantity	$D' = 1/2$, $\theta = \pi/2$	$D' = 1/2$, $\theta = 0$	$D' = 1$, $\theta = 0$	T dep.
$I_{\mathrm{A}_1^+}$, $I_{\mathrm{A}_1^-}$	$\frac{e}{\mathcal{T}}\left(\frac{1}{4}+\frac{R}{2}\right)$	$\frac{e}{\mathcal{T}}\left(\frac{1}{4}+\frac{R}{2}\right)$	$\frac{e}{\mathcal{T}}\left(\frac{1}{4}+\frac{R}{2}\right)$	1
$I_{\mathrm{A}_2^+}$, $I_{\mathrm{A}_2^-}$	$\frac{e}{\mathcal{T}}\left(\frac{1}{4}+\frac{D}{2}\right)$	$\frac{e}{\mathcal{T}}\left(\frac{1}{4}+\frac{D}{2}\right)$	$\frac{e}{\mathcal{T}}\left(\frac{1}{4}+\frac{D}{2}\right)$	1
I_{B_1}, I_{B_2}	$\frac{e}{2\mathcal{T}}$	$\frac{e}{2\mathcal{T}}$	$\frac{e}{2\mathcal{T}}$	1
$\mathcal{P}_{\mathrm{A}_1^\pm\mathrm{A}_2^\pm}$	$-\frac{e^2RD}{4\mathcal{T}}$	$-\frac{e^2RD}{4\mathcal{T}}$	$-\frac{e^2RD}{4\mathcal{T}}$	$F(T)$
$\mathcal{P}_{\mathrm{A}_1^+\mathrm{B}_1}$, $\mathcal{P}_{\mathrm{A}_2^+\mathrm{B}_2}$	$-\frac{e^2}{16\mathcal{T}}$	$-\frac{e^2}{16\mathcal{T}}$	$-\frac{e^2}{8\mathcal{T}}$	$F(T)$
$\mathcal{P}_{\mathrm{A}_1^+\mathrm{A}_1^-}$, $\mathcal{P}_{\mathrm{A}_2^+\mathrm{A}_2^-}$	$-\frac{e^2}{\mathcal{T}}\left(\frac{1}{16}-\frac{RD}{4}\right)$	$-\frac{e^2}{\mathcal{T}}\left(\frac{1}{16}-\frac{RD}{4}\right)$	$-\frac{e^2}{\mathcal{T}}\left(\frac{1}{16}-\frac{RD}{4}\right)$	$F(T)$
$\mathcal{P}_{\mathrm{A}_1^+\mathrm{B}_2}$, $\mathcal{P}_{\mathrm{A}_2^+\mathrm{B}_1}$	$-\frac{e^2}{16\mathcal{T}}$	$-\frac{e^2}{16\mathcal{T}}$	0	$F(T)$
$\mathcal{Q}_{\mathrm{A}_1^+\mathrm{A}_2^+\mathrm{B}_1}$	$\frac{e^3}{\mathcal{T}}\frac{\sqrt{RD}\sin\varphi}{16}$	$-\frac{e^3}{\mathcal{T}}\frac{\sqrt{RD}\cos\varphi}{16}$	0	$A(T)$
$\mathcal{Q}_{\mathrm{A}_1^+\mathrm{A}_2^+\mathrm{B}_2}$	$-\frac{e^3}{\mathcal{T}}\frac{\sqrt{RD}\sin\varphi}{16}$	$\frac{e^3}{\mathcal{T}}\frac{\sqrt{RD}\cos\varphi}{16}$	0	$A(T)$
$\mathcal{Q}_{\mathrm{A}_1^+\mathrm{A}_1^-\mathrm{A}_2^+}$	$\frac{e^3}{\mathcal{T}}\frac{RD(R-D)}{8}$	$\frac{e^3}{\mathcal{T}}\frac{RD(R-D)}{8}$	$\frac{e^3}{\mathcal{T}}\frac{RD(R-D)}{8}$	$A(T)$
$\mathcal{Q}_{\mathrm{A}_1^+\mathrm{A}_2^+\mathrm{A}_2^-}$	$\frac{e^3}{\mathcal{T}}\frac{RD(D-R)}{8}$	$\frac{e^3}{\mathcal{T}}\frac{RD(D-R)}{8}$	$\frac{e^3}{\mathcal{T}}\frac{RD(D-R)}{8}$	$A(T)$

The functions F and A that determine the temperature dependence of the second and third order correlators can be evaluated numerically, and are shown in Figure 4.1 for different values of $\Gamma\Omega$. From those plots we see that both the second and third order correlators will approach zero as temperature increases, although $\mathcal{Q}_{\alpha\beta\gamma}$ will go to zero more rapidly than $\mathcal{P}_{\alpha\beta}$. The plots also indicate that if we keep Ω fixed, then decreasing Γ will keep the correlators closer to their zero temperature values for a larger temperature span, although at zero temperature the values are independent of Γ.

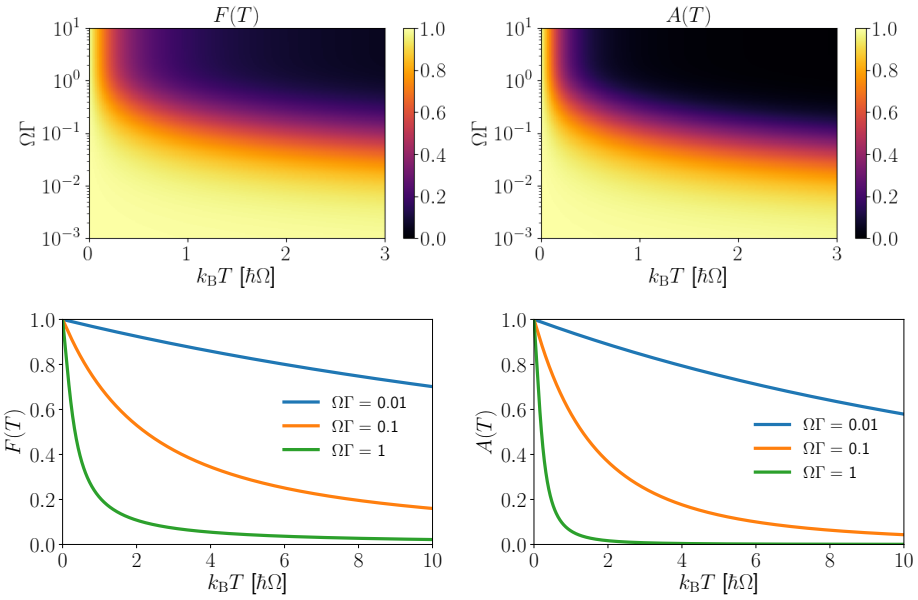

Figure 4.1: Temperature dependence of the second and third order correlators.

4.2.3 Zero temperature results

As can be seen from Figure 4.1, $F(T)$ and $A(T)$ approach 1 as $T \to 0$. Mathematically this can be seen either by taking the limit $k_BT/\hbar\Omega \to 0$ in Eqs. (4.25) and (4.30), or by replacing $f(E)$ with the step function $\theta(-E)$ when calculating the integrals $\chi(n-m)$ and $G(n-k, s-k)$. From Table 4.1 and Alice and Bob's combined pre-measurement state, Eq. (3.9), we can verify that the correspondence that was derived in Section 4.2.1 holds. This means that it is possible to perform a teleportation experiment with levitons that relies on measurements of I_α, $\mathcal{P}_{\alpha\beta}$ and $\mathcal{Q}_{\alpha\beta\gamma}$ instead of relying on single-electron detection. It should be noted that we need to assume that the settings of the leviton sources, width and period, are such that only levitons from the same period are traveling in the leads at the same time. Then it becomes possible to interpret the periodic application of the pulses as repeatedly teleporting single leviton states. To make the correspondence between the Floquet correlators and tomography observables concrete, we can write out Bob's Bloch vector corresponding to when Alice measures $++$, in terms of the correlators

$$r_i' = \left.\frac{J}{K}\right|_{T=0}, \tag{4.31}$$

where we have defined

$$\begin{aligned}J =&\frac{\mathcal{T}}{e^3}\Big(\mathcal{Q}_{\mathrm{A}_1^+\mathrm{A}_2^+\mathrm{B}_1}-\mathcal{Q}_{\mathrm{A}_1^+\mathrm{A}_2^+\mathrm{B}_2}\Big)+\frac{\mathcal{T}^2}{e^3}\Big(\mathcal{P}_{\mathrm{A}_1^+\mathrm{A}_2^+}(I_{\mathrm{B}_1}-I_{\mathrm{B}_2})+I_{\mathrm{A}_2^+}(\mathcal{P}_{\mathrm{A}_1^+\mathrm{B}_1}-\mathcal{P}_{\mathrm{A}_1^+\mathrm{B}_2})+\\&+I_{\mathrm{A}_1^+}(\mathcal{P}_{\mathrm{A}_2^+\mathrm{B}_1}-\mathcal{P}_{\mathrm{A}_2^+\mathrm{B}_2})\Big)+\frac{\mathcal{T}^3}{e^3}I_{\mathrm{A}_1^+}I_{\mathrm{A}_2^+}\Big(I_{\mathrm{B}_1}-I_{\mathrm{B}_2}\Big),\\K =&\frac{\mathcal{T}^2}{e^2}I_{\mathrm{A}_1^+}I_{\mathrm{A}_2^+}\Big(1-\frac{\mathcal{T}}{e}(I_{\mathrm{A}_1^-}+I_{\mathrm{A}_2^-})\Big)-\frac{\mathcal{T}^2}{e^3}\Big(I_{\mathrm{A}_1^+}(\mathcal{P}_{\mathrm{A}_1^-\mathrm{A}_2^+}+\mathcal{P}_{\mathrm{A}_2^+\mathrm{A}_2^-})+\\&+I_{\mathrm{A}_2^+}(\mathcal{P}_{\mathrm{A}_1^+\mathrm{A}_1^-}+\mathcal{P}_{\mathrm{A}_1^+\mathrm{A}_2^-})\Big)-\frac{\mathcal{T}}{e^3}\Big(\mathcal{Q}_{\mathrm{A}_1^+\mathrm{A}_2^+\mathrm{A}_1^-}+\mathcal{Q}_{\mathrm{A}_1^+\mathrm{A}_2^+\mathrm{A}_2^-}\Big).\end{aligned} \tag{4.32}$$

J and K are found by applying the correspondence derived in Section 4.2.1 to the numerator and denominator, respectively, of Eq. (4.6). This means that K corresponds to the probability that the outcome $++$ is found by Alice. If the $T = 0$ values from Table 4.1 are plugged in to the above expressions we find $r_i' = r_i$. We now have enough to be able to verify that teleportation is possible to perform using levtions in QHE edge modes.

4.2.4 Finite temperature results

At finite temperatures the simple picture of teleportation that has been presented so far becomes problematic, since our system will contain thermal excitations in addition to the levitons. This means that the POVM that was defined in Eq. (4.1) is no longer appropriate to describe the situation, since it only accounts for the presence of levitons. If there are additional excitations present, it is not guaranteed that $\langle N_i \rangle$ is bounded between zero and one, which in turn would mean that the POVM elements can become negative. If the operators defined in Eq. (4.1) are no longer positive, then they do not define a POVM. Furthermore, we can no longer rigorously justify Eq. (4.8) since it was derived under the assumption that there are only three electrons in the system. However, we can still calculate the quantity on the right-hand side of Eq. (4.31) at finite temperatures. This can be used to define a new Bloch vector with components $\widetilde{r}_i$,

$$\widetilde{r}_i = \frac{J}{K}\bigg|_{T\geq 0}, \tag{4.33}$$

which at $T = 0$ will correspond to the Bloch vector of Bob's state if Alice measures $++$. At low temperatures, where the number of additional excitations is small, one might still expect Eq. (4.33) to be a good approximation to the correct picture, but showing that requires a more careful argument. These additional excitations also mean that we strictly speaking no longer have a qubit system, since the excitations makes our state a more complicated many-body state.

Nevertheless, we can still discuss how $\vec{\widetilde{r}}$ behaves at nonzero temperature, to investigate the deviations of the zero temperature scenario. Computing $\widetilde{r}_i$ gives

$$\vec{\widetilde{r}} = \begin{bmatrix} q(T)r_x \\ q(T)r_y \\ r_z \end{bmatrix}, \tag{4.34}$$

where $q(T) = A(T)/F(T)$. $q(T)$ is plotted in Figure 4.2 and those plots suggest that q behaves similarly to A and F, although it does not decrease as rapidly with temperature

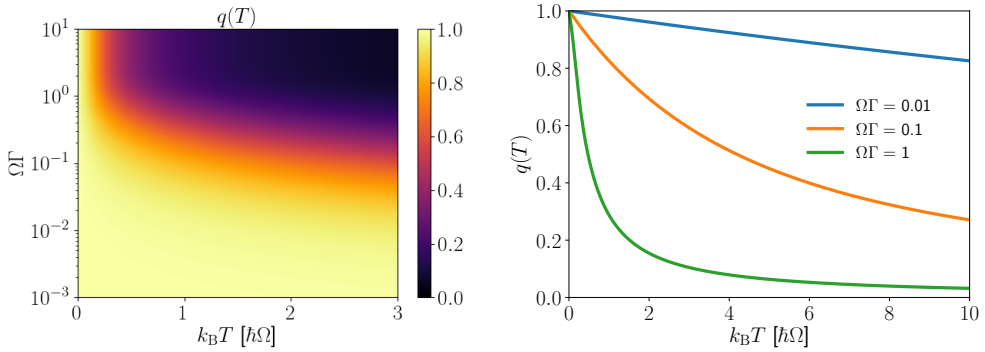

Figure 4.2: Temperature dependence of $q(T)$ for different values of $\Gamma\Omega$.

as A and F. The x and y components of the Bloch vector will shrink towards the center of the Bloch sphere since they are multiplied by $q(T)$, but the z-component is unaffected. The prepared states satisfy the equation $r_x^2 + r_y^2 + r_z^2 = 1$, because they are pure states, but teleported states instead describe the surface

$$\frac{\widetilde{r}_x^2 + \widetilde{r}_y^2}{q(T)^2} + \widetilde{r}_z^2 = 1, \tag{4.35}$$

which for $q(T) < 1$ is a prolate spheroid. Some examples of transformed Bloch spheres for a few different values of $\Gamma\Omega$ and $k_\mathrm{B}T/\hbar\Omega$ are presented in Figure 4.3. Included in each figure is the Bloch vector $(0, -1/\sqrt{2}, 1/\sqrt{2})$ and the corresponding $\vec{\widetilde{r}}$ Bloch vector. From these figures we see that the regions around the north and south poles of the Bloch sphere contain the states that are least affected when the temperature is increased. These are the states that are almost fully in one of the two modes. A prolate spheroid possesses a cylindrical symmetry along the z-axis, in that each slice orthogonal to the z-axis, i.e. where R and D are constant, will be described by a circle. This suggests that some interesting quantities such as purity and fidelity might not have a φ dependence. If we also assume that K is a low temperature approximation of the probability for $++$ outcomes in Alice's measurement, then we see that the probability will be $F(T)/16$, which decreases as temperature increases. In terms of teleportation, this suggests that the probability for successful teleportation is negatively affected by an increase in temperature, but a rigorous argument requires a proper POVM.

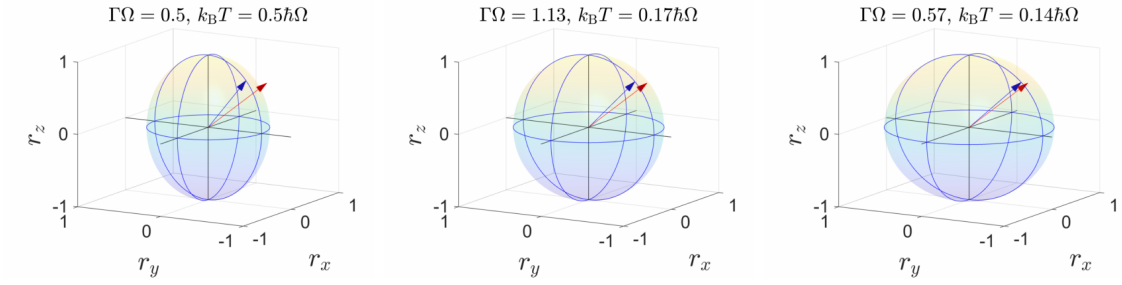

Figure 4.3: Here we can see how the Bloch sphere transforms as we move to finite temperatures. $\vec{r}$ and $\vec{\widetilde{r}}$ are represented by the red and blue vectors, respectively. In the last two pictures, the parameters were taken from an experiment that was performed with levitons [37].

A transformation of the Bloch vector like the one in Eq. 4.34 can be viewed as if a random change in the phase difference of a superposition state has occured. This type of noise can be described by a proccess called a phase flip, where the phase factor of one of the basis states changes sign with some probability p [7]. Since the north and south poles of the Bloch sphere are not superpositions of modes, they are unaffected by this type of noise. On the other hand, states on the equator are equal superpositions of two modes and information about the superposition is lost when the phase is altered, which leads to a less pure state. Since only the x and y components of the Bloch vector are affected, this type of noise will transform the Bloch sphere into ellipsoids, as is shown in Figure 4.3. So $\vec{\tilde{r}}$ seems to describe a teleported version of the state described by $\vec{r}$ having been disturbed by some phase noise. Again, we should be careful about drawing too many conclusions from these calculations, since our identification of $\vec{\tilde{r}}$ with a Bloch vector is not rigorous, but should rather be seen as a way to investigate deviations from the ideal, zero temperature behavior.

Taking this analogy to noisy teleportation further, we can use the results of Section 2.2 to calculate the purity of the teleported state, as well as the teleportation fidelity. The purity of the teleported qubit will be

$$\gamma = \frac{1 + q(T)^2\,(4RD) + (R - D)^2}{2}, \tag{4.36}$$

and is shown as a function of temperature for a few different values of R and $\Gamma\Omega$ in Figure 4.4. The plots tell us that as the temperature increases the purity will decrease until it reaches a constant value. Equation (4.36) suggests that what value the purity will approach depends on R. If R is close to 0 or 1, then γ will be closer to 1, but if R is close to $1/2$, γ will instead approach values close to $1/2$. If $\gamma = 1/2$, then the state is completely mixed. This point is well illustrated in the left panel of Figure 4.4. On the other hand, the right-hand panel shows that the leviton width is very important in determining the purity of the output state, since there is a very large difference between the three different cases. This is not surprising when one considers that $q(T)$ also depends very strongly on $\Omega\Gamma$, as shown in Figure 4.2. The reason that we get better values for the purity when $\Gamma\Omega$ is small is that the energy distribution for the leviton is broader, see e.g. Eqs. (2.62) and (2.63), which means that the levitons stand out more from the Fermi sea, which will have thermal excitations with energies of order $k_{\mathrm{B}}T$ around the Fermi energy.

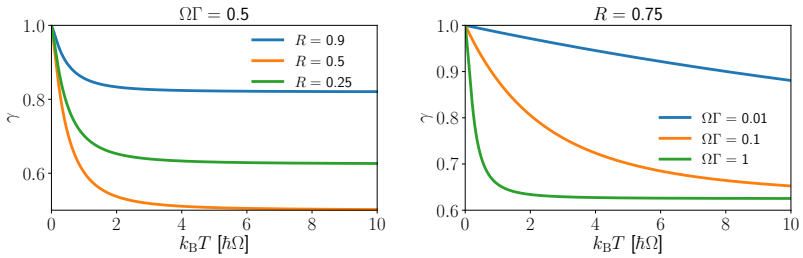

Figure 4.4: These plots show the purity γ of the teleported state as a function of temperature. On the left we have chosen a specific width of the levitons and the different lines correspond to the purity of the teleported state for different values of R for the original state. On the right we have instead chosen a specific value of R and varied the width of the levitons.

The fidelity between the states described by the $\vec{r}$ and $\vec{\tilde{r}}$ Bloch vectors is

$$\mathcal{F}\left(\rho,\tilde{\rho}\right)=\frac{1+4q(T)RD+(R-D)^2}{2}. \tag{4.37}$$

One thing to notice here is that neither the purity nor the fidelity depends on the relative phase between the two modes that make up the qubit, since the expressions for both γ and $\mathcal{F}$ do not contain φ. This is a manifestation of the cylindrical symmetry that is present in the Bloch sphere transformations that the finite temperature introduces. Therefore, we do not have to consider φ when calculating the teleportation fidelity. Averaging $\mathcal{F}$ over R, and using $D=1-R$, leads to a teleportation fidelity of the form

$$\mathcal{F}_{\text{tel}}=\frac{2}{3}+\frac{q(T)}{3}. \tag{4.38}$$

From this we see that the teleporation fidelity approaches the classical limit of $2/3$ as the temperature is increased, as Figure 4.5 illustrates. However, $\mathcal{F}_{\text{tel}}$ always lies above the classical limit. This is perhaps not so surprising considering that according to Eq. 4.33, the fidelity should be perfect for the classical states, i.e. those with no superpositions. The classical strategy for teleportation mentioned in Section 2.2 is unaffected by the phase noise discussed above since the probability of finding one of the basis states is independent of the relative phase.

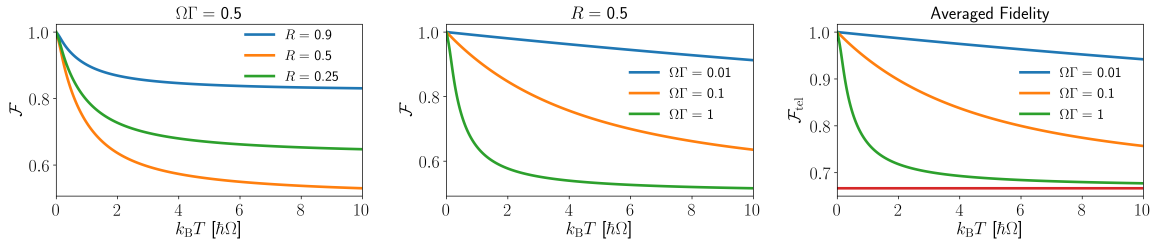

Figure 4.5: These plots show the fidelity between the input state and the output state as a function of the temperature. In the left panel we consider a fixed leviton width for different input states. In the middle panel, we consider a fixed input state for different leviton widths. The right panel shows $\mathcal{F}_{\text{tel}}$, i.e. the fidelity of the input and output states averaged over all possible input states. This is plotted for different leviton widths and is compared to the best possible fidelity of a classical teleportation scheme (horizontal line).

To get some feeling for what values of $\Omega\Gamma$ and at what temperatures it is currently realistic to operate at, we can consider the experiment [37] which generated and studied levitons. One part of the experiment was performed at $T=39\,\text{mK}$ and used two pairs of values for Ω and Γ, $\Omega=2\pi\cdot4.8\,\text{GHz}$, $\Gamma=37.5\,\text{ps}$, $\Omega\Gamma=1.13$ and $\Omega=2\pi\cdot6\,\text{GHz}$, $\Gamma=15\,\text{ps}$, $\Omega\Gamma=0.57$. Table 4.2 contains the $\mathcal{F}_{\text{tel}}$ values that we find using these parameters, along with the remaining parameter pair used in Figure 4.3. The results in Table 4.2 say that with realistic operating parameters we could measure a fidelity close to 1, having neglected of course other sources of noise such as electron-electron interactions. Such interactions might for instance occur between levitons from adjacent pulses, or between the levitons and the rest of the 2DEG.

Table 4.2: Values of the teleportation fidelity for the same parameters used in Figure 4.3

$k_{\mathrm{B}}T/\hbar\Omega$	$\Omega\Gamma$	$\mathcal{F}_{\mathrm{tel}}$
0.5	0.5	0.88
0.17	1.13	0.93
0.14	0.57	0.96

To see if the assumption of well separated pulses is satisfied for the values of $\Gamma\Omega$ that have been used in this section, we can look at the corresponding pulse trains to see how much the individual pulses overlap. As Figure 4.6 shows, for $\Omega\Gamma = 0.01$ and 0.1 the individual pulses are well separated, while for $\Omega\Gamma = 1$ the pulses overlap to a greater extent. Since the values of $\Omega\Gamma$ that were taken from experiment are in the latter range, it would be good if the leviton width in experiments could be decreased further, in order for the assumption of well separated levitons to be valid.

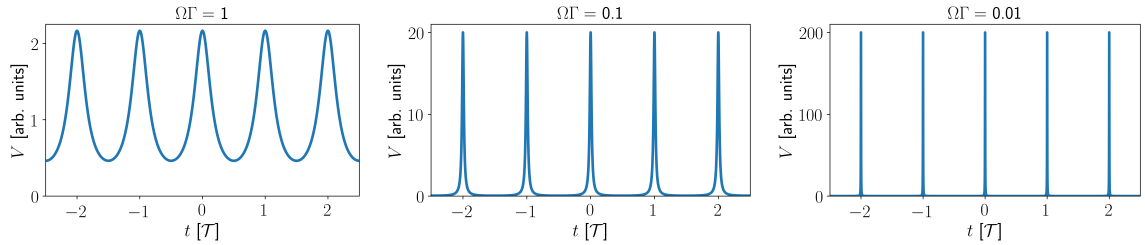

Figure 4.6: Examples of Lorentizan pulse trains showing the mount of overlap between individual pulses. As the width of the indivudal pulses are increased, the assumption that the pulses are well separated becomes less justified.

Chapter 5

Summary and outlook

The results of this thesis project show that it is possible to perform quantum teleportation using single-electron states. This was done by working within the framework of electron quantum optics. We demonstrated two possible experiments that realize quantum teleportation. The first one requires reliable single-electron detection for flying qubits, which have not yet been demonstrated for systems based on edges states in the QHE. A scheme to perform quantum state tomography on the teleported state was also described. The second experiment where we periodically create levitons and do not perform single-electron detection but instead measure average currents and zero frequency current cross correlators, is currently the more realistic approach if one wants to work with architectures based on edge states for guiding the electrons. In the periodically driven case we also studied how the situation changes when non-zero temperatures are considered. The work performed during this thesis is intended to be a part of a future journal publication.

In the single-shot experiment, teleportation is successful 25% of the time, provided a conditional unitary transformation based on the outcome of Alice's measurement is implemented by Bob. If the transformation is not included, the efficiency is instead 12,5%. The protocol we have presented is probabilistic even in the best case scenario, and a challenge for other quantum information protocols that are constructed similarly to our experiment, if the aim is to create a useful system, is to minimize the probability of ending up with an unwanted outcome.

The usefulness of the second experiment, lies in the fact that we can perform state tomography and find success probabilities with measurements of direct currents and zero frequency current cross correlators instead of single-electron detection. For a levtion and QHE architecture, single-electron detection is not yet available, and this experiment is therefore more feasible to perform than the idealized version. Still, the experiment is not completely straightforward to perform since it requires 20 different quantities to be measured, see Table 4.1. The periodic injection experiment serves as a proof of concept for single-electron teleportation and possible applications of periodic leviton teleportation have not been considered.

In the finite temperature case it is still possible to write down a Bloch vector, $\vec{\tilde{r}}$, in terms of the correlators that are used at zero temperature. $\vec{\tilde{r}}$ will look like the Bloch vector of the original state affected by noise. As was stated in the text, precisely how one should interpret the state represented by $\vec{\tilde{r}}$ is not fully understood, since the addition of thermal excitations means that the POVM that was defined for the ideal case can fail at nonzero temperatures, because the POVM elements are no longer guaranteed to be positive. This means that $\vec{\tilde{r}}$ might not represent a quantity of the same form as Eq. (4.8).

One could hope that the expression for $\vec{\tilde{r}}$ can be derived as a low temperature limit from a description of the teleportation setup that properly deals with the additional excitations. In other words, since Eq. (4.31) is exact at $T = 0$, one can perhaps show that Eq. (4.33) should be a good description at low temperatures, where the effects of thermal excitations should be small. Showing such a result would require additional work and has not been done in this thesis.

There are several ways to connect the results of this thesis to a bigger picture. First, we have demonstrated a new system in which we can perform quantum teleportation. One can argue that it is not perhaps an extremely useful approach since the efficiency is not as high as others and the distances over which teleporation can be performed are not very large, a few µm, compared to some of the alternatives presented in Chapter 1. However, quantum information experiments with single electrons is a fairly new topic and studying basic systems can be thought of as proof of principle experiments, with the aim of trying to determine if there are applications where a single-electron approach can be appropriate. As a part of this, one has to also consider which of the physical systems that have been discussed here are most suitable for these kinds of tasks. This thesis has focused mostly on levitons traveling in edge channels, but SAW based approaches has the advantage that there single-electron detection is more straightforward. One also has to consider other parameters such as the electron coherence length and how easy the systems are to fabricate.

Another way is to think of this as a stepping stone to other technologies that utilize electron quantum optics. Teleportation is one of the simpler protocols within quantum information processing, and we can try to build upon it to perform more complex tasks. For instance one could study the entanglement swapping protocol mentioned in Chapter 1, or perhaps investigate architectures that have been proposed for optical quantum computation. More broadly one can study how to utilize control over single-electron states in other types of technologies. From a theorists point of view, this would involve analyzing experiments that can be performed with the tools available to experimentalists.

Bibliography

[1] C. H. Bennett, G. Brassard, C. Crépeau, R. Jozsa, A. Peres, and W. K. Wootters. Teleporting an unknown quantum state via dual classical and Einstein-Podolsky-Rosen channels. *Phys. Rev. Lett.*, 70:1895–1899, Mar 1993.

[2] M. Żukowski, A. Zeilinger, M. A. Horne, and A. K. Ekert. "Event-ready-detectors" Bell experiment via entanglement swapping. *Phys. Rev. Lett.*, 71:4287–4290, Dec 1993.

[3] S. Pirandola, J. Eisert, C. Weedbrook, A. Furusawa, and S. L. Braunstein. Advances in quantum teleportation. *Nat. Photon.*, 9:641–652, Sep 2015.

[4] H.-J. Briegel, W. Dür, J. I. Cirac, and P. Zoller. Quantum repeaters: The role of imperfect local operations in quantum communication. *Phys. Rev. Lett.*, 81:5932–5935, Dec 1998.

[5] D. Gottesman and I. L. Chuang. Demonstrating the viability of universal quantum computation using teleportation and single-qubit operations. *Nature*, 402:390–393, Nov 1999.

[6] E. Knill, R. Laflamme, and G.J. Milburn. A scheme for efficient quantum computation with linear optics. *Nature*, 409(6816):46–52, Jan 2001.

[7] M. A. Nielsen and I. L. Chuang. *Quantum Computation and Quantum Information*. Cambridge University Press, Cambridge, 10th anniversary edition, Dec 2010.

[8] D. Bouwmeester, J.-W. Pan, K. Mattle, M. Eibl, H. Weinfurter, and A. Zeilinger. Experimental quantum teleportation. *Nature*, 390:575–579, Dec 1997.

[9] E. Lombardi, F. Sciarrino, S. Popescu, and F. De Martini. Teleportation of a Vacuum–One-Photon Qubit. *Phys. Rev. Lett.*, 88:070402, Jan 2002.

[10] I. Marcikic, H. de Riedmatten, W. Tittel, H. Zbinden, and N. Gisin. Long-distance teleportation of qubits at telecommunication wavelengths. *Nature*, 421:509–513, Jan 2003.

[11] M. D. Barrett, J. Chiaverini, T. Schaetz, J. Britton, W. M. Itano, J. D. Jost, E. Knill, C. Langer, D. Leibfried, R. Ozeri, and D. J. Wineland. Deterministic quantum teleportation of atomic qubits. *Nature*, 429:737–739, Jun 2004.

[12] M. A. Nielsen, E. Knill, and R. Laflamme. Complete quantum teleportation using nuclear magnetic resonance. *Nature*, 396:52–55, Nov 1998.

[13] L. Steffen, Y. Salathe, M. Oppliger, P. Kurpiers, M. Baur, C. Lang, C. Eichler, G. Puebla-Hellmann, A. Fedorov, and A. Wallraff. Deterministic quantum teleportation with feed-forward in a solid state system. *Nature*, 500:319–322, Aug 2013.

[14] J.-G. Ren, P. Xu, H.-L. Yong, L. Zhang, S.-K. Liao, J. Yin, W.-Y. Liu, W.-Q. Cai, M. Yang, L. Li, K.-X. Yang, X. Han, Y.-Q. Yao, J. Li, H.-Y. Wu, S. Wan, L. Liu, D.-Q. Liu, Y.-W. Kuang, Z.-P. He, P. Shang, C. Guo, R.-H. Zheng, K. Tian, Z.-C. Zhu, N.-L. Liu, C.-Y. Lu, R. Shu, Y.-A. Chen, C.-Z. Peng, J.-Y. Wang, and J.-W. Pan. Ground-to-satellite quantum teleportation. *Nature*, 549:70–73, Sep 2017.

[15] E. Bocquillon, V. Freulon, F. D. Parmentier, J.-M. Berroir, B. Placais, C. Wahl, J. Rech, T. Jonckheere, T. Martin, C. Grenier, D. Ferraro, P. Degiovanni, and G. Fève. Electron quantum optics in ballistic chiral conductors. *Ann. Phys.*, 526(1-2):1–30, Jan 2014.

[16] C. Bäuerle, D. C. Glattli, T. Meunier, F. Portier, P. Roche, P. Roulleau, S. Takada, and X. Waintal. Coherent control of single electrons: a review of current progress. *Rep. Prog. Phys.*, 81:056503, Apr 2018.

[17] P. P. Hofer, D. Dasenbrook, and C. Flindt. On-demand entanglement generation using dynamic single-electron sources. *Phys. Status Solidi B*, 254:1600582, Mar 2017.

[18] D. Dasenbrook, J. Bowles, J. B. Brask, P. P. Hofer, C. Flindt, and N. Brunner. Single-electron entanglement and nonlocality. *New J. Phys.*, 18:043036, Apr 2016.

[19] M. V. Moskalets. *Scattering matrix approach to non-stationary quantum transport.* Imperial College Press, London, 2012.

[20] E. Witten. A Mini-Introduction To Information Theory. arXiv:1805.11965v4 [hep-th], Dec 2018.

[21] R. Jozsa. Fidelity for Mixed Quantum States. *J. Mod. Opt.*, 41(12):2315–2323, 1994.

[22] V. Kashcheyevs and P. Samuelsson. Classical-to-quantum crossover in electron on-demand emission. *Phys. Rev. B*, 95:245424, Jun 2017.

[23] D. Tong. Lectures on the Quantum Hall Effect. arXiv:1606.06687v2 [hep-th], Sep 2016.

[24] M. Büttiker. Absence of backscattering in the quantum Hall effect in multiprobe conductors. *Phys. Rev. B*, 38:9375–9389, Nov 1988.

[25] P. Zanardi. Quantum entanglement in fermionic lattices. *Phys. Rev. A*, 65:042101, Mar 2002.

[26] R. Thalineau, A. D. Wieck, C. Bäuerle, and T. Meunier. Using a two-electron spin qubit to detect electrons flying above the fermi sea. arXiv:1403.7770 [cond-mat.mes-hall], Mar 2014.

[27] H. Goldstein, C. P. Poole, and J. Safko. *Classical mechanics.* Pearson, Harlow, third edition, 2014.

[28] M. E. Peskin and D. V. Schroeder. *An introduction to quantum field theory.* Addison-Wesley, Reading, Mass., 1995.

[29] Y. M. Blanter and M. Büttiker. Shot noise in mesoscopic conductors. *Phys. Rep.*, 336:1–166, Sep 200.

[30] T. Bilitewski and N. R. Cooper. Scattering theory for Floquet-Bloch states. *Phys. Rev. A*, 91:033601, Mar 2015.

[31] E. Merzbacher. *Quantum mechanics*. Wiley, New York, third edition, 1998.

[32] P. P. Hofer. *Dynamic Mesoscopic Conductors: Single Electron Sources, Full Counting Statistics, and Thermal Machines*. PhD thesis, University of Geneva, 2016.

[33] M. Büttiker. Quantized transmission of a saddle-point constriction. *Phys. Rev. B*, 41:7906–7909, Apr 1990.

[34] L. D. Landau, E. M. Lifshitz, and L. P. Pitaevskij. *Statistical physics. P. 2, Theory of the condensed state*. Pergamon, Oxford, second edition, 1980.

[35] L. S. Levitov, H. Lee, and G. B. Lesovik. Electron counting statistics and coherent states of electric current. *J. Math. Phys.*, 37(10):4845–4866, 1996.

[36] J. Keeling, I. Klich, and L. S. Levitov. Minimal Excitation States of Electrons in One-Dimensional Wires. *Phys. Rev. Lett.*, 97:116403, Sep 2006.

[37] J. Dubois, T. Jullien, F. Portier, P. Roche, A. Cavanna, Y. Jin, W. Wegscheider, P. Roulleau, and D. C. Glattli. Minimal-excitation states for electron quantum optics using levitons. *Nature*, 502:659–663, Oct 2013.

[38] M. Moskalets and G. Haack. Single-electron coherence: Finite temperature versus pure dephasing. *Physica E*, 75:358 – 369, 2016.

[39] C. W. J. Beenakker and M. Kindermann. Quantum Teleportation by Particle-Hole Annihilation in the Fermi Sea. *Phys. Rev. Lett.*, 92:056801, Feb 2004.

[40] P. Samuelsson and M. Büttiker. Quantum state tomography with quantum shot noise. *Phys. Rev. B*, 73:041305, Jan 2006.

[41] P. Samuelsson, E. V. Sukhorukov, and M. Büttiker. Two-Particle Aharonov-Bohm Effect and Entanglement in the Electronic Hanbury Brown–Twiss Setup. *Phys. Rev. Lett.*, 92:026805, Jan 2004.

[42] H.-S. Sim and E. V. Sukhorukov. Multiparticle Interference, Greenberger-Horne-Zeilinger Entanglement, and Full Counting Statistics. *Phys. Rev. Lett.*, 96:020407, Jan 2006.

[43] O. M. Corbino. *Atti accad. nazl. Lincei*, 20:(342, 416, 569, 746), 1911.

[44] D. A. Kleinman and A. L. Schawlow. Corbino Disk. *J. Appl. Phys.*, 31(12):2176–2187, Dec 1960.

[45] J. Dubois, T. Jullien, C. Grenier, P. Degiovanni, P. Roulleau, and D. C. Glattli. Integer and fractional charge Lorentzian voltage pulses analyzed in the framework of photon-assisted shot noise. *Phys. Rev. B*, 88:085301, Aug 2013.

Appendix A

Checking beamsplitter and phase settings for state tomography

We represent the qubit

$$|\psi\rangle = (\alpha a^{\dagger}_{\mathrm{B}'_1} + \beta a^{\dagger}_{\mathrm{B}'_2})\,|0\rangle \tag{A.1}$$

by the vector

$$\begin{bmatrix}\alpha\\ \beta\end{bmatrix}. \tag{A.2}$$

The expectation values for $\sigma_{x,y}$ are given by

$$r_x = \langle\psi|\,\sigma_x\,|\psi\rangle = \begin{bmatrix}\alpha^* & \beta^*\end{bmatrix}\begin{bmatrix}0 & 1\\ 1 & 0\end{bmatrix}\begin{bmatrix}\alpha\\ \beta\end{bmatrix} = \alpha^*\beta + \alpha\beta^* \tag{A.3}$$

and

$$r_y = \langle\psi|\,\sigma_y\,|\psi\rangle = \begin{bmatrix}\alpha^* & \beta^*\end{bmatrix}\begin{bmatrix}0 & -i\\ i & 0\end{bmatrix}\begin{bmatrix}\alpha\\ \beta\end{bmatrix} = -i\alpha^*\beta + i\alpha\beta^*. \tag{A.4}$$

In the B_1 and B_2 basis, the state is represented by the vector

$$\begin{bmatrix}\sqrt{D'}e^{-i\theta} & -i\sqrt{R'}\\ -i\sqrt{R'}e^{-i\theta} & \sqrt{D'}\end{bmatrix}\begin{bmatrix}\alpha\\ \beta\end{bmatrix} = \begin{bmatrix}\sqrt{D'}e^{-i\theta}\alpha - i\sqrt{R'}\beta\\ -i\sqrt{R'}e^{-i\theta}\alpha + \sqrt{D'}\beta\end{bmatrix}. \tag{A.5}$$

The expectation value of σ'_z is

$$\begin{aligned}&\begin{bmatrix}(\sqrt{D'}e^{i\theta}\alpha^* + i\sqrt{R'}\beta^*) & (i\sqrt{R'}e^{i\theta}\alpha^* + \sqrt{D'}\beta^*)\end{bmatrix}\begin{bmatrix}1 & 0\\ 0 & -1\end{bmatrix}\begin{bmatrix}\sqrt{D'}e^{-i\theta}\alpha - i\sqrt{R'}\beta\\ -i\sqrt{R'}e^{-i\theta}\alpha + \sqrt{D'}\beta\end{bmatrix} =\\ &= D'|\alpha|^2 - i\sqrt{R'D'}e^{i\theta}\alpha^*\beta + i\sqrt{R'D'}e^{-i\theta}\alpha\beta^* + R'|\beta|^2 - R'|\alpha|^2 - ie^{i\theta}\sqrt{R'D'}\alpha^*\beta +\\ &+ ie^{-i\theta}\sqrt{R'D'}\alpha\beta^* - D'|\beta|^2.\end{aligned} \tag{A.6}$$

If the expression after the last equality sign is evaluated for $R' = D' = 1/2$ it reduces to

$$i\left(e^{-i\theta}\alpha\beta^* - e^{i\theta}\alpha^*\beta\right). \tag{A.7}$$

With $\theta = \pi/2$ this expression is equal to r_x and with $\theta = 0$ it is equal to r_y.

Appendix B

Verifying the POVM

A general POVM element describing the detection of the particle number of each mode at A is given by

$$E\left(j_{\mathrm{A}_1^+}, j_{\mathrm{A}_1^-}, j_{\mathrm{A}_2^+}, j_{\mathrm{A}_2^-}\right) = \prod_i N_i^{j_i} \left(I - N_i\right)^{(1-j_i)}, \tag{B.1}$$

where $j_i \in \{0, 1\}$ is the number of electrons detected in mode i, with $i \in \{\mathrm{A}_1^+, \mathrm{A}_1^-, \mathrm{A}_2^+, \mathrm{A}_2^-\}$. $N_i = a_i^\dagger a_i$ is the particle number operator for mode i. The factor $N_i^{j_i} \left(I - N_i\right)^{(1-j_i)}$ in the POVM will project states onto the subspace with j_i particles in mode i. For the POVM elements used in the main text we have $E(+,+) = E(1,0,1,0)$ etc. That the operators defined by Eq. (B.1) are positive follows from the fact that they are products of operators with eigenvalues 0 and 1 on the occupation number basis. Explicit examples of elements with four, three, two, one and zero particles detected are

$$E(1,1,1,1) = N_{\mathrm{A}_1^+} N_{\mathrm{A}_1^-} N_{\mathrm{A}_2^+} N_{\mathrm{A}_2^-},$$

$$E(1,1,1,0) = N_{\mathrm{A}_1^+} N_{\mathrm{A}_1^-} N_{\mathrm{A}_2^+} \left(I - N_{\mathrm{A}_2^-}\right),$$

$$E(1,0,1,0) = N_{\mathrm{A}_1^+} N_{\mathrm{A}_2^+} \left(I - N_{\mathrm{A}_1^-}\right)\left(I - N_{\mathrm{A}_2^-}\right) = N_{\mathrm{A}_1^+} N_{\mathrm{A}_2^+} \left(I - N_{\mathrm{A}_1^-} - N_{\mathrm{A}_2^-} + N_{\mathrm{A}_1^-} N_{\mathrm{A}_2^-}\right),$$

$$E(1,0,0,0) = N_{\mathrm{A}_1^+} \left(I - N_{\mathrm{A}_1^-}\right)\left(I - N_{\mathrm{A}_2^+}\right)\left(I - N_{\mathrm{A}_2^-}\right) = N_{\mathrm{A}_1^+} \Big(I - N_{\mathrm{A}_1^-} - N_{\mathrm{A}_2^+} - N_{\mathrm{A}_2^-} +$$
$$+ N_{\mathrm{A}_1^-} N_{\mathrm{A}_2^+} + N_{\mathrm{A}_1^-} N_{\mathrm{A}_2^-} + N_{\mathrm{A}_2^+} N_{\mathrm{A}_2^-} - N_{\mathrm{A}_1^-} N_{\mathrm{A}_2^+} N_{\mathrm{A}_2^-}\Big),$$

$$E(0,0,0,0) = \left(I - N_{\mathrm{A}_1^+}\right)\left(I - N_{\mathrm{A}_1^-}\right)\left(I - N_{\mathrm{A}_2^+}\right)\left(I - N_{\mathrm{A}_2^-}\right) = \Big(I - N_{\mathrm{A}_1^+} - N_{\mathrm{A}_1^-} - N_{\mathrm{A}_2^+} -$$
$$- N_{\mathrm{A}_2^-} + N_{\mathrm{A}_1^+} N_{\mathrm{A}_1^-} + N_{\mathrm{A}_1^+} N_{\mathrm{A}_2^+} + N_{\mathrm{A}_1^+} N_{\mathrm{A}_2^-} + N_{\mathrm{A}_1^-} N_{\mathrm{A}_2^+} + N_{\mathrm{A}_1^-} N_{\mathrm{A}_2^-} + N_{\mathrm{A}_2^+} N_{\mathrm{A}_2^-} -$$
$$- N_{\mathrm{A}_1^+} N_{\mathrm{A}_1^-} N_{\mathrm{A}_2^+} - N_{\mathrm{A}_1^+} N_{\mathrm{A}_1^-} N_{\mathrm{A}_2^-} - N_{\mathrm{A}_1^+} N_{\mathrm{A}_2^+} N_{\mathrm{A}_2^-} - N_{\mathrm{A}_1^-} N_{\mathrm{A}_2^+} N_{\mathrm{A}_2^-} + N_{\mathrm{A}_1^+} N_{\mathrm{A}_1^-} N_{\mathrm{A}_2^+} N_{\mathrm{A}_2^-}\Big).$$

The remaining elements will simply be index permutations of one of these five. When the elements are written out in the form above, a straightforward calculation shows that

$$\sum_X E(X) = I,$$

with $X \in \{(j_{\mathrm{A}_1^+}, j_{\mathrm{A}_1^-}, j_{\mathrm{A}_2^+}, j_{\mathrm{A}_2^-})\}$. We have now demonstrated that this set of operators are positive and sum to the identity and can therefore conclude that they form a POVM.

Appendix C

Derivation of the third order correlator

Since the relation between the Bloch vector components of the teleported state and the current correlators involve a third order current cross correlator between currents at A and B, we need to find an expression for $\mathcal{Q}_{\alpha\beta\gamma}$ that can be evaluated. This expression is valid under the assumptions that α, β and γ are not equal and that the system is chiral in the sense that electrons are created at the sources and travel towards the outputs.

To start with we need to define $Q_{\alpha\beta\gamma}$ and find an expression for it in terms of Floquet scattering matrix elements. This can be done by calculating the correlator $\langle \hat{I}_\alpha(\omega_1)\hat{I}_\beta(\omega_2)\hat{I}_\gamma(\omega_3)\rangle$, where the $\hat{I}_\alpha(\omega_i)$ are current operators in frequency space. The correlator can be expressed in terms of average currents and fluctuation operators, $\Delta\hat{I}_\alpha = \hat{I}_\alpha - \langle\hat{I}_\alpha\rangle$, as

$$\begin{aligned}\langle \hat{I}_\alpha(\omega_1)\hat{I}_\beta(\omega_2)\hat{I}_\gamma(\omega_3)\rangle = \langle\hat{I}_\alpha\rangle\langle\hat{I}_\beta\rangle\langle\hat{I}_\gamma\rangle + \langle\hat{I}_\alpha\rangle\langle\Delta\hat{I}_\beta\Delta\hat{I}_\gamma\rangle + \langle\hat{I}_\beta\rangle\langle\Delta\hat{I}_\alpha\Delta\hat{I}_\gamma\rangle + \\ + \langle\hat{I}_\gamma\rangle\langle\Delta\hat{I}_\alpha\Delta\hat{I}_\beta\rangle + \langle\Delta\hat{I}_\alpha\Delta\hat{I}_\beta\Delta\hat{I}_\gamma\rangle,\end{aligned} \tag{C.1}$$

by using $\langle\Delta\hat{I}_\alpha\rangle = 0$. The left-hand side of Eq. (C.1) can also be expressed in terms of creation and annihilation operators by using the frequency space expression for the current in lead α

$$\hat{I}_\alpha(\omega) = e\int_{-\infty}^{\infty} \mathrm{d}E\left(b_\alpha^\dagger(E)b_\alpha(E+\hbar\omega) - a_\alpha^\dagger(E)a_\alpha(E+\hbar\omega)\right). \tag{C.2}$$

This will lead to an expression that involves calculating averages of products of six creation and annihilation operators and there are eight such terms. Wick's theorem says that we can compute the average of a product of creation and annihilation operators, by computing the sum of products of expaction values of paired operators [34]. For example Wick's theorem says that

$$\begin{aligned}\langle a_\alpha^\dagger a_\alpha a_\beta^\dagger a_\beta a_\gamma^\dagger a_\gamma\rangle = \langle a_\alpha^\dagger a_\alpha\rangle\langle a_\beta^\dagger a_\beta\rangle\langle a_\gamma^\dagger a_\gamma\rangle + \langle a_\alpha^\dagger a_\alpha\rangle\langle a_\beta^\dagger a_\gamma\rangle\langle a_\beta a_\gamma^\dagger\rangle + \\ + \langle a_\alpha^\dagger a_\beta\rangle\langle a_\alpha a_\beta^\dagger\rangle\langle a_\gamma^\dagger a_\gamma\rangle - \langle a_\alpha^\dagger a_\beta\rangle\langle a_\alpha a_\gamma^\dagger\rangle\langle a_\beta^\dagger a_\gamma\rangle + \\ + \langle a_\alpha^\dagger a_\gamma\rangle\langle a_\alpha a_\gamma^\dagger\rangle\langle a_\beta^\dagger a_\gamma\rangle + \langle a_\alpha^\dagger a_\gamma\rangle\langle a_\alpha a_\gamma^\dagger\rangle\langle a_\beta^\dagger a_\beta\rangle.\end{aligned}$$

The sign of each term above is determined by the number of operator swaps needed to go from the original product to the new one. Wick's theorem can be applied to express Eq. (C.1) in terms of these sums. It is then possible to identify terms that make up the first four terms of the right-hand side of Eq. (C.1) and the remaining terms make up

$\langle \Delta\hat{I}_\alpha \Delta\hat{I}_\beta \Delta\hat{I}_\gamma \rangle$. The result is

$$\begin{aligned}\langle \Delta\hat{I}_\alpha \Delta\hat{I}_\beta \Delta\hat{I}_\gamma \rangle = e^3 \int_{-\infty}^{\infty}\int_{-\infty}^{\infty}\int_{-\infty}^{\infty} \mathrm{d}E_1 \mathrm{d}E_2 \mathrm{d}E_3 \Big(&- \langle b_\alpha^\dagger b_\beta\rangle\langle b_\alpha b_\gamma^\dagger\rangle\langle b_\beta^\dagger b_\gamma\rangle + \\ &+ \langle b_\alpha^\dagger b_\gamma\rangle\langle b_\alpha b_\beta^\dagger\rangle\langle b_\beta b_\gamma^\dagger\rangle + \langle b_\alpha^\dagger b_\beta\rangle\langle b_\alpha a_\gamma^\dagger\rangle\langle b_\beta^\dagger a_\gamma\rangle - \langle b_\alpha^\dagger a_\gamma\rangle\langle b_\alpha b_\beta^\dagger\rangle\langle b_\beta a_\gamma^\dagger\rangle + \\ &+ \langle b_\alpha^\dagger a_\beta\rangle\langle b_\alpha b_\gamma^\dagger\rangle\langle a_\beta^\dagger b_\gamma\rangle - \langle b_\alpha^\dagger b_\gamma\rangle\langle b_\alpha a_\beta^\dagger\rangle\langle a_\beta b_\gamma^\dagger\rangle - \langle b_\alpha^\dagger a_\beta\rangle\langle b_\alpha a_\gamma^\dagger\rangle\langle a_\beta^\dagger a_\gamma\rangle + \\ &+ \langle b_\alpha^\dagger a_\gamma\rangle\langle b_\alpha a_\beta^\dagger\rangle\langle a_\beta a_\gamma^\dagger\rangle + \langle a_\alpha^\dagger b_\beta\rangle\langle a_\alpha b_\gamma^\dagger\rangle\langle b_\beta^\dagger b_\gamma\rangle - \langle a_\alpha^\dagger b_\gamma\rangle\langle a_\alpha b_\beta^\dagger\rangle\langle b_\beta b_\gamma^\dagger\rangle - \\ &- \langle a_\alpha^\dagger b_\beta\rangle\langle a_\alpha a_\gamma^\dagger\rangle\langle b_\beta^\dagger a_\gamma\rangle + \langle a_\alpha^\dagger a_\gamma\rangle\langle a_\alpha b_\beta^\dagger\rangle\langle b_\beta a_\gamma^\dagger\rangle - \langle a_\alpha^\dagger a_\beta\rangle\langle a_\alpha b_\gamma^\dagger\rangle\langle a_\beta^\dagger b_\gamma\rangle + \\ &+ \langle a_\alpha^\dagger b_\gamma\rangle\langle a_\alpha a_\beta^\dagger\rangle\langle a_\beta b_\gamma^\dagger\rangle + \langle a_\alpha^\dagger a_\beta\rangle\langle a_\alpha a_\gamma^\dagger\rangle\langle a_\beta^\dagger a_\gamma\rangle - \langle a_\alpha^\dagger a_\gamma\rangle\langle a_\alpha a_\beta^\dagger\rangle\langle a_\beta a_\gamma^\dagger\rangle \Big).\end{aligned} \tag{C.3}$$

Here E_1 is the energy associated with the α operators, E_2 with the β operators and E_3 with the γ operators.

We can now use Eqs. (2.45) and (2.41) to calculate each of the terms above. Fortunately most of the terms will vanish for the system we are considering. First the Kronecker deltas in Eq. (2.45) removes any term containing an average over incoming electrons from different leads, this will be true for any system where incoming electrons from different reservoirs are assumed to be uncorrelated. The fact that we are using chiral edge states to implement the scheme then removes any term containing averages of the form $\langle b_\alpha^\dagger a_\beta\rangle$ and $\langle b_\alpha a_\beta^\dagger\rangle$ with α and β both detectors, since by Eqs. (2.45) and (2.41) they will be proportional to $S_F(E_m, E_n)_{\alpha\beta}$, or its complex conjugate, and such matrix elements are zero when both α and β are detectors. This is a result of the absence of backscattering which is a feature of the chiral edge states. The result of this is that only the first two terms in Eq. (C.3) are non-zero, and so the amount of calculation needed is reduced greatly.

The first term in Eq. (C.3) written in terms of matrix elements and distribution functions and with two of the delta functions integrated away is

$$\begin{aligned}&\sum_{\delta,\varepsilon,\zeta}\sum_{k,l,n,s,u,v=-\infty}^{\infty} 2\pi\delta(l\Omega-\omega_1-\omega_2-\omega_3)\frac{e^3}{h}\int_{-\infty}^{\infty}\mathrm{d}E f(E_n)\left(1-f(E_s+\hbar\omega_1)\right) \\ &f(E_k+\hbar(\omega_1+\omega_3))S_F^*(E,E_n)_{\alpha\delta}S_F(E_{k-u}+\hbar(\omega_1+\omega_2+\omega_3),E_{n-l}+\hbar(\omega_1+\omega_2+\omega_3))_{\beta\delta} \\ &S_F(E+\hbar\omega_1,E_s+\hbar\omega_1)_{\alpha\varepsilon}S_F^*(E_{k-v}+\hbar\omega_1,E_s+\hbar\omega_1)_{\gamma\varepsilon} \\ &S_F^*(E_{k-u}+\hbar(\omega_1+\omega_3),E_k+\hbar(\omega_1+\omega_3))_{\beta\zeta}S_F(E_{k-v}+\hbar(\omega_1+\omega_3),E_k+\hbar(\omega_1+\omega_3))_{\gamma\zeta}.\end{aligned} \tag{C.4}$$

Doing the same for the second term gives

$$\begin{aligned}&\sum_{\delta,\varepsilon,\zeta}\sum_{k,l,n,s,u,v=-\infty}^{\infty} 2\pi\delta(l\Omega-\omega_1-\omega_2-\omega_3)\frac{e^3}{h}\int_{-\infty}^{\infty}\mathrm{d}E f(E_n)\left(1-f(E_s+\hbar\omega_1)\right) \\ &\left(1-f(E_k+\hbar(\omega_1+\omega_2))\right)S_F^*(E,E_n)_{\alpha\delta}S_F(E_{k-v}+\hbar(\omega_1+\omega_2+\omega_3),E_{n-l}+\hbar(\omega_1+\omega_2+\omega_3))_{\gamma\delta} \\ &S_F(E+\hbar\omega_1,E_s+\hbar\omega_1)_{\alpha\varepsilon}S_F^*(E_{k-u}+\hbar\omega_1,E_s+\hbar\omega_1)_{\beta\varepsilon} \\ &S_F(E_{k-u}+\hbar(\omega_1+\omega_2),E_k+\hbar(\omega_1+\omega_2))_{\beta\zeta}S_F^*(E_{k-v}+\hbar(\omega_1+\omega_2),E_k+\hbar(\omega_1+\omega_2))_{\gamma\zeta}.\end{aligned} \tag{C.5}$$

What we are interested in is the zero frequency part of the two expressions above,

which corresponds to $\omega_i = 0$ and $l = 0$. This is given by

$$\begin{aligned}\mathcal{Q}_{\alpha\beta\gamma} = \frac{e^3}{h}\sum_{\delta,\varepsilon,\zeta}\sum_{k,n,s,u,v=-\infty}^{\infty}\Big(&-h(n,s,k)S_F^*(E,E_n)_{\alpha\delta}S_F(E_{k-u},E_n)_{\beta\delta}\\ &\times S_F(E,E_s)_{\alpha\varepsilon}S_F^*(E_{k-v},E_s)_{\gamma\varepsilon}S_F^*(E_{k-u},E_k)_{\beta\zeta}S_F(E_{k-v},E_k)_{\gamma\zeta}+\\ &+g(n,s,k)S_F^*(E,E_n)_{\alpha\delta}S_F(E_{k-v},E_n)_{\gamma\delta}S_F(E,E_s)_{\alpha\varepsilon}S_F^*(E_{k-u},E_s)_{\beta\varepsilon}\\ &\times S_F(E_{k-u},E_k)_{\beta\zeta}S_F^*(E_{k-v},E_k)_{\gamma\zeta}\Big).\end{aligned} \tag{C.6}$$

where h and g are defined by

$$\begin{aligned}h(n,s,k) &= \int_{-\infty}^{\infty}\mathrm{d}E f(E_n)\left(1-f(E_s)\right)f(E_k),\\ g(n,s,k) &= \int_{-\infty}^{\infty}\mathrm{d}E f(E_n)\left(1-f(E_s)\right)\left(1-f(E_k)\right).\end{aligned} \tag{C.7}$$

Using some simple algebra, one can show $h(s,n,k) = g(-n,-s,-k)$. The function $g(n,s,k)$ is also clearly invariant under a simultaneous translation of all three variables i.e. $g(n,s,k) = g(n+a,s+a,k+a)$ with $a \in \mathbb{R}$. This means that we can write $g(n,s,k) = G(n-k,s-k)$, that is g only depends on the differences $n-k$ and $s-k$. So the final result is

$$\begin{aligned}\mathcal{Q}_{\alpha\beta\gamma} = \frac{e^3}{h}\sum_{\delta,\varepsilon,\zeta}\sum_{k,n,s,u,v=-\infty}^{\infty}\Big(&-G(k-n,k-s)S_F^*(E,E_n)_{\alpha\delta}S_F(E_{k-u},E_n)_{\beta\delta}\\ &\times S_F(E,E_s)_{\alpha\varepsilon}S_F^*(E_{k-v},E_s)_{\gamma\varepsilon}S_F^*(E_{k-u},E_k)_{\beta\zeta}S_F(E_{k-v},E_k)_{\gamma\zeta}+\\ &+G(n-k,s-k)S_F^*(E,E_n)_{\alpha\delta}S_F(E_{k-v},E_n)_{\gamma\delta}S_F(E,E_s)_{\alpha\varepsilon}S_F^*(E_{k-u},E_s)_{\beta\varepsilon}\\ &\times S_F(E_{k-u},E_k)_{\beta\zeta}S_F^*(E_{k-v},E_k)_{\gamma\zeta}\Big).\end{aligned} \tag{C.8}$$